1-1-2002

Characterization of phase transformations for Mo-Si-B system around T1 phase region

Yang Sui
Iowa State University

Characterization of phase transformations for Mo-Si-B system around T1 phase region

by

Yang Sui

A thesis submitted to the graduate faculty

in partial fulfillment of the requirements for the degree of

MASTER OF SCIENCE

Major: Materials Science and Engineering

Program of Study Committee:
Mufit Akinc, (Major Professor)
Matthew J. Kramer
Gordon Miller

Iowa State University

Ames, Iowa

2002

Graduate College
Iowa State University

This is to certify that the master's thesis of

Yang Sui

has met the thesis requirements of Iowa State University

Signatures have been redacted for privacy

TABLE OF CONTENTS

ABSTRACT

Previous investigation on the Mo-Si-B phase diagram was reviewed. Six Mo-Si-B samples around T1 region were studied to characterize phase transformations using chemical analysis, X-ray diffraction analysis, differential thermal analysis, and scanning electron microscopy. The studies were focused on two ternary phase transformations, III: $L \rightarrow Mo + T2 + Mo_3Si$, and IV: $L \rightarrow T1 + T2 + Mo_3Si$. Previous confusion about the nature of reaction IV was clarified to be eutectic reaction. Phase transition temperatures were determined to be 1924±3°C and 1938±3 °C for reaction III and IV, respectively. Heat of phase transition for III and IV was calculated from DTA measurement to be 5.95×10^5J/kg and 8.99×10^5J/kg, respectively.

It is particularly important to solve the containment problem in ultrahigh temperature DTA instrument prior to the phase transition studies for Mo-Si-B system. Yttria-stabilized zirconia was found to be a satisfactory liner material to protect tungsten crucible in that it was compatible with Mo-Si-B samples, while maintaining the validity of the DTA measurement.

Nitrogen was determined to be the only suitable inert atmosphere for carrying out ultrahigh temperature DTA experiments because it helped stabilize the type C thermocouples. The reason might be a nitride layer was formed on the surface of thermocouples to prevent evaporation of thermocouple material at ultrahigh temperature. Argon and helium have been discovered to be improper as inert atmosphere since they caused thermocouple drift.

CHAPTER 1: INTRODUCTION

1.1 Oxidation and mechanical properties of molybdenum silicides

Currently there is a need for a new class of materials that can withstand higher temperatures for applications such as next generation heat exchangers or power generators. Greater efficiency can be achieved if the devices can be operated at a higher temperature. Advanced materials for service at high temperature, such as 1600°C, must combine strength, creep resistance, fracture toughness, and oxidation resistance over the temperature range between room temperature and the maximum service temperature [1].

One family of such compounds being investigated for high temperature application is the intermetallics. Intermetallics are a large class of compounds composed of two or more metals or combinations of metals and metalloids. They typically exhibit properties between metals and ceramics, and are generally brittle at low temperatures while being ductile at elevated temperatures. Intermetallics are actually thermodynamically unstable at high temperatures compared to the parent metal oxides, but the ability of some of these materials to form a passivating adherent oxide layer, which acts as a barrier to further oxygen diffusion, can make them oxidation-resistant. As an important class of intermetallics, silicides tend to form a passivating SiO_2 layer at elevated temperatures. [1]
Currently, silicides are being investigated as possible candidate materials for use in high temperature (>1100°C) oxidizing environments because of their unique ability to form a glassy SiO_2 protective layer when oxidized. As long as the glass layer is adherent to the underlying material, it prevents further oxidation of the materials underneath.

Of the silicides, $MoSi_2$ has by far received the most attention due to its excellent oxidation resistance, high melting temperature (T_m=2020°C), and moderately low density of 6.24 g/cm^3. $MoSi_2$ is well known to have a good oxidative stability up to 1700°C in air environment due to the formation of a passivating SiO_2 coating. However, monolithic $MoSi_2$, in single crystal and polycrystalline forms, has a high temperature ductile-to-brittle transition temperature of 1000°C and is simply not adequate for structural applications because of its poor strength and brittleness at low temperatures and insufficient high temperature creep resistance. [1]

At temperatures ranging from 400-600°C, $MoSi_2$ shows catastrophic oxidation behavior resulting in pesting, which is basically caused by simultaneous oxidation of Mo and Si [2].

Fitzer et al [4] concluded that pesting phenomenon was not an intrinsic property of $MoSi_2$ and that it required the presence of initial microcracks and pores in the material.

It is indicated by Kurokawa et al [1] that cracks initiate from the surface or edge of specimen and propagate inwardly, resulting in pesting. Water vapor also accelerates the pesting of $MoSi_2$. However, the influence of H_2O can be sufficiently suppressed by using fully dense $MoSi_2$ without defects on the surface, which further demonstrates the necessity of defects in the pesting of $MoSi_2$ [2].

$MoSi_2$ has a high oxidation resistance at high temperatures. Reaction

$$2MoSi_2 + 7O_2 \rightarrow 2MoO_3 + 4\ SiO_2$$

occurs at temperatures lower than 1000°C. Reaction

$$5MoSi_2 + 7O_2 \rightarrow Mo_5Si_3 + 7SiO_2$$

prevails at higher temperatures. Oxidative stability of $MoSi_2$, following initial oxidation of surface at moderate temperatures ($400<T<600$°C), depends on the temperature range that it is subjected to. At $T>750$°C, MoO_3 volatilizes leaving behind a layer of SiO_2 on the surface of $MoSi_2$, which effectively prevents diffusion of oxygen from attacking the $MoSi_2$ underneath. At $T<700$°C, MoO_3 does not volatilize and the oxide layer is highly porous, providing an easy passage for oxygen diffusion, which ultimately leads to pesting [3].

Yanagihara et al [11] studied the effects of ternary elements on pesting, and showed that the third elements with higher affinity to oxygen than silicon effectively prevented pest disintegration.

Although $MoSi_2$ has excellent oxidation resistance at temperature from 1000°C to 1700°C in air, it has a high creep rate above 1200°C, making it unsuitable as a high temperature structural material. Mo_5Si_3, on the other hand, has a very large and complex unit cell, which contains four formula units. A large and complex unit cell, with a large Burger's vector, is the reason that researchers consider Mo_5Si_3 would have a better creep resistance than $MoSi_2$ [1]. Meyer et al verified this by creep experiments and found that the creep rate of Mo_5Si_3 is at least an order of magnitude lower than that of the published values for $MoSi_2$ [6].

The melting temperature of Mo_5Si_3, which is 2180°C, has been found to be higher than $MoSi_2$. The oxidation resistance of Mo_5Si_3 has generally been reported to be unacceptable for high-temperature use in air. It is characterized by porous scale formation and oxidative loss of Mo below about 1650°C. [4]

Bartlett et al explained the oxidation of Mo by the partial pressure of oxygen at the oxidation interface [5]. The model is based on the premise that, in order to maintain P_{O2} at the level thermodynamically indicated by Si/SiO_2 equilibria, the rate of Si supply to the oxidation interface must be faster than the rate of Si consumption due to reaction with O_2. If the Si supply rate is slower than Si consumption rate, the oxidation interface become silicon-depleted and oxygen partial pressure at interface increases. An increasing in P_{O2} will lead to oxidation of Mo and volatilization as MoO_3, causing the scale to rupture and become non-passivating [5]. At higher temperatures, Si diffusion rate is sufficiently high and no Mo is oxidized. A protective SiO_2 layer is formed.

At lower temperatures ranging from 600-1000°C, it has been shown by Meyer et al that doping 1-2 wt% boron significantly improves the oxidation resistance of Mo_5Si_3 by several orders of magnitude [6]. Mechanism of high oxidation resistance of boron-doped Mo_5Si_3 is also explained by Meyer et al. At 600°C, the scale is composed of three distinct areas: small pockets of borosilicate glass and almost pure MoO_3 are surrounded by a matrix of mixed molybdenum and silicon oxides. At 633°C, larger MoO_3 crystals begin to form around "pure" MoO_3. At 750°C, MoO_3 begins to sublime, which leads to the decrease of both number and size of MoO_3 crystals. At 775°C, MoO_3 crystals cover half the surface and the remainder is composed of porous borosilicate glass. Viscous flow starts at 1000°C and then a coherent protective layer is formed.

Oxygen pressure at oxidation interface, porosity and viscosity are the keys for forming a protective layer. If oxidation is limited by oxygen diffusion, oxygen partial pressure will be fixed by the Si/SiO_2 equilibria. SiO_2 has a much lower free energy of formation than any molybdenum oxide. The dominant oxidation reaction will be:

$$Mo_5Si_3 + 3O_2 \rightarrow 5Mo + 3SiO_2$$

A silicon-depleted and molybdenum rich interlayer will thus form.

On the other hand, if the partial pressure of oxygen at the interface is high enough to oxidize molybdenum, the following reaction is expected to occur::

$2Mo_5Si_3 + 21O_2 \rightarrow 10\ MoO_3$ (volatile) $+ 6SiO_2$.

The reaction predicts a mass loss due to volatilization of MoO_3. A metallic Mo interlayer will not form.

When viscous flow doesn't close pores, porosity of the layer determines the steady state oxidation rate. When viscous flow forms a coherent layer, oxidation is controlled by diffusion rate of oxygen through the layer [6].

Another important molybdenum silicide, Mo_5SiB_2 also has a high melting temperature of over 2100°C. In order to study the solid-liquid phase transformation, the instrument must have the capability of over 2200 °C.

1.2 Phase diagrams of Mo-Si-B system

Nowotny et al studied the Mo-Si-B system during their research into the stabilizing

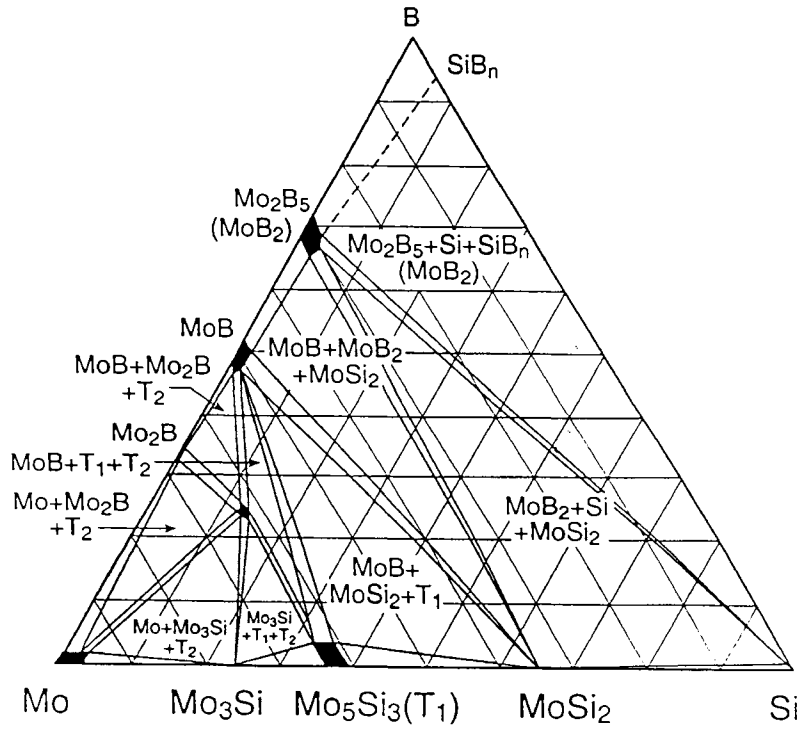

Fig 1.1 Isotherm at 1600°C of Mo-Si-B ternary phase diagram [7]

effects of small dopant atoms on the crystal structure of $Mo_{5+y}Si_{3-y}$ [7]. Their work generated the 1600°C isotherm of Mo-Si-B system. However, due to the fact that they employed fairly low purity starting materials, the accuracy of the published isotherm is in question.

It has been shown elsewhere [6] that boron-doped Mo_5Si_3 can reach an oxidation resistance comparable to that of $MoSi_2$. This boron-doped Mo_5Si_3 generally doesn't show catastrophic oxidation at intermediate temperature, except that Summers et al indicated that T1-$MoSi_2$-MoB (70vol% T1, 20vol% $MoSi_2$, and 10vol% MoB) samples showed pesting behavior between 660°C-760°C [28].

The creep strength of Mo_5Si_3 is superior to that of $MoSi_2$. However, the fracture toughness of alloys in Mo_3Si-T1 (Mo_5Si_3)-T2 (Mo_5SiB_2) system is likely to be low [12]. The alloys consisting of α-Mo, Mo_3Si and T2 have higher fracture toughness than the Mo_3Si-T1-T2 alloys because of the presence of α-Mo. However, their oxidation resistance is lower for the same reason [12]. It is likely that the oxidation resistance can be improved by minimizing the α-Mo volume fraction, by suitable alloying additions or silicide coatings[13].

Fig 1.2 shows the single phase T1 region in the Mo-Si-B diagram at 1800°C as determined by Huebsch et al [1]. The dashed line represents the T1 region from the Nowotny 1600°C diagram [7] as a reference. The single phase region (shaded region) is based on

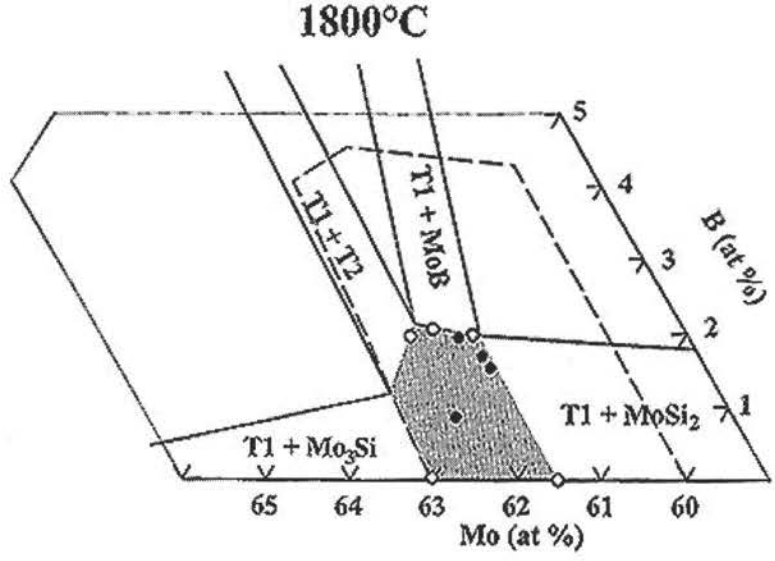

Fig 1.2 Experimentally determined T1 region at 1800°C.
The shaded region is determined by EPMA

EPMA results for the Mo/Si, while boron solubility limit is determined from single phase samples based on XRD and initial starting composition [14].

In order to achieve equilibrium at 1800°C, samples were annealed up to 92 hours. Although the heat treatment promoted the equilibrium condition, the significant vapor pressure of Si at this temperature shifts the T1 composition to Mo rich side. The homogeneity range for T1 phase was determined to be 61.5-62.9 at% Mo and 1-2 at% B. The maximum solubility for B occurs at 62.0 at% Mo content [15]. It was found that Nowotny's phase assemblages still hold true around T1, however, the single phase region was much smaller than the 1600°C isotherm [7,14].

Study of phase stability of Mo-Si-B alloys in high temperature by Nunes et al gave a liquidus projection for Mo-rich side of the Mo-Si-B system [16]. The projection (Fig 1.3) gave quite a good idea about the shape of the liquidus surface on Mo_3Si-MoB-Mo_5Si_3 region. However, the Mo-Mo_3Si-T2 region, of which the material exhibits superior mechanical properties, does not have many data points. This may be due to experimental difficulties that Mo-rich region is very refractory. Furthermore, phase diagram does not show liquidus boundaries or phase transitions in detail.

The liquidus projection for Mo-rich side of the Mo-B-Si system was constructed by Nunes et al [16]. In their experiments, melted samples were cast in a copper crucible, and the microstructure of the as-cast alloys is examined by SEM (Scanning Electron Microscope) to identify the primary phase. The solidification path was also determined basically from studying the BSEI (Back-scattered Electron Image) of the as-cast alloys. The positions of the univariant lines were determined by narrowing down the compositions of the samples and studying the primary phase of these as-cast samples by SEM [16]. This approach to determine the univariant lines positions may limit the precision of the result because only finite number of compositions can be studied which may not be enough to determine the exact position of the univariant lines. The cast samples could also differ from the high temperature equilibrium composition.

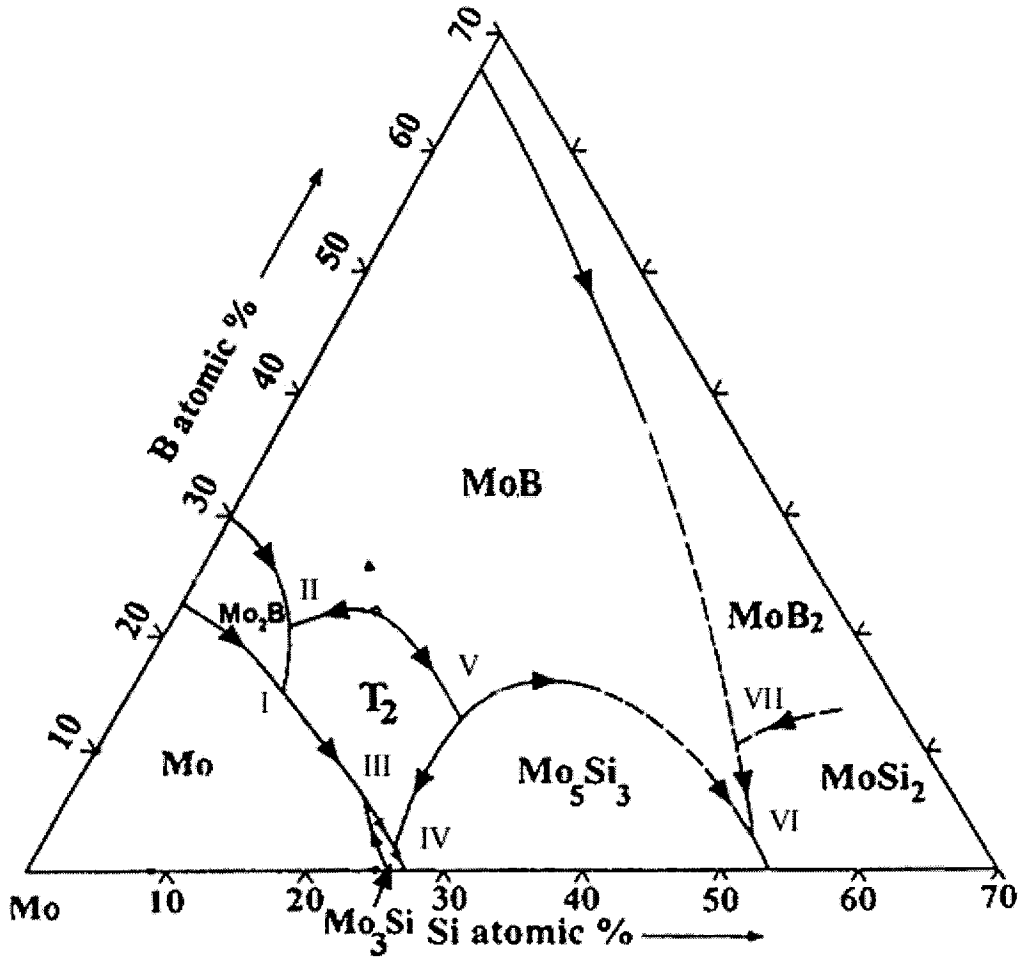

Fig 1.3 Liquidus projection for Mo-rich side of the Mo-B-Si system [16]

Seven ternary solidification reactions are indicated in Nunes' work. They are:

I: $Mo_2B + L \rightarrow Mo + T2$

II: $MoB + L \rightarrow Mo_2B + T2$

III: $L \rightarrow Mo + T2 + Mo_3Si$

IV: $T1 + L \rightarrow Mo_3Si + T2$

V: $MoB + L \rightarrow T1 + T2$

VI: $MoB + L \rightarrow T1 + MoSi_2$

VII: $MoB_2 + L \rightarrow MoB + MoSi_2$

1.3 Differential thermal analysis of Mo-Si-B

Differential thermal analysis (DTA) is a very effective method for studying phase transformation and phase diagram since most phase transitions are associated with heat exchange. DTA measures the temperature difference between a sample and a reference material as a function of temperature while the sample and reference are subjected to a controlled temperature program [8].

DTA has a number of advantages: solid, liquid and gel samples in the shape of powder, films, fabric, etc. are applicable; only small amount of sample is required; the time required for measurement is relatively short; the atmosphere in the vicinity of sample can be defined; sample can be annealed, aged or cured and their previous thermal history can be erased in thermal analysis (TA) measurements [8].

However, DTA also has some drawbacks: the observed transition temperature represents a non-equilibrium state; the precise temperature and temperature gradient in the sample is unknown. [8]

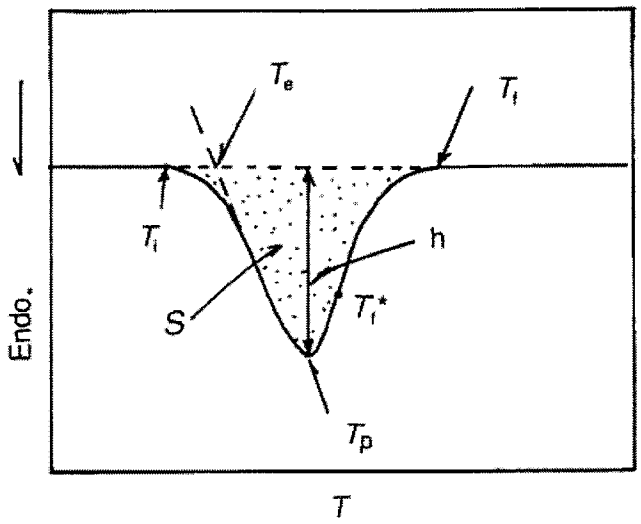

Fig 1.4 Schematic DTA curve of chemical reaction or physical transition [8]

A typical DTA curve is shown in Fig 1.4. T_i, T_e, T_p and T_f are initial temperature, extrapolated onset temperature, peak temperature and final temperature for the reaction, respectively. T_e usually has a relatively good repeatability and is considered the transition temperature. The peak height h is proportional to the reaction rate and the peak area S is proportional to the reaction heat.

Experimental conditions have profound effects on the DTA output. Heating rate influences the temperature gradient in the sample. The temperature difference inside and outside the sample is minimum when heating rate is very slow (2.5°C/min), and it could be as large as 10°C when the heating rate is 40°C/min. Heating rate is an important factor in determining the phase transition point [8]. In a DTA test, the transition temperature shift to the high temperature side with increasing heating rate. The peak area also decreases with decreasing heating rate [17].

The slower heating rate is, the closer the system is to equilibrium. However, slow heating rate introduces a number of problems. First, a slower heating/cooling rate gives a smaller peak in DTA curve [24]. The peak will be eventually too small to be identified with decreasing heating/cooling rate. Second, a slower heating/cooling rate will expose the specimen to elevated temperature for longer time, which may cause specimen evaporation and result in the change of composition. If the oxygen or water vapor pressure in the inert atmosphere is not well controlled, slower heating/cooling rate may also cause oxidation of specimen, which may change the phase transition temperature [9].

For the DTA tests of the Mo-Si-B samples used in this investigation, since the sample size is very small (dimension < 3mm), small amount of water vapor or oxygen may significantly alter the results. Therefore, a high vacuum ($<10^{-6}$ torr) is required to evacuate the chamber prior to each run.

The onset transition temperature for the heating curve is more accurate than the one for the cooling curve. Significant undercooling tends to indicate much lower reaction equilibrium temperature. Since some phase transitions are very sluggish, even under very slow heating rate, onset equilibrium phase transition point cannot be directly measured from DTA data. Some mathematical extrapolation methods are used to determine the equilibrium phase transition temperature from the measured data.

$T = C \bullet S^{1/3} + T_0$ [9] or $T = C \bullet S + T_0$

where C is constant, S is heating rate(°C/min), T is measured transition temperature and T_0 is equilibrium transition temperature. Only several T and S values are needed to obtain a linear extrapolation and determine T_0. [9]

Mass and particle size also affect DTA measurement. Temperature gradient exists within samples. According to the study by Zhu et al [9], the temperature difference between a point in the sample and the center of the sample, ΔT is given by:

$$\Delta T = -\frac{S(b^2 - r^2)}{6\kappa}$$

where S is heating/cooling rate, b is sample radius, r is the distance from specimen center to the specific point, κ is thermal diffussivity of the sample under investigation [9].
When the size of sample is small, the temperature difference between the surface of sample and the center is small. Thus the above correction becomes negligible. Surrounding atmosphere also makes the temperature of the sample uniform and reduce the temperature difference between sample and sample holder.

The peak area A, is dependent on the mass of sample m, heat change of the reaction or transition ΔH, and thermal conductivity *k* [8]:

$$A = \frac{G \bullet m \bullet \Delta H}{k}$$

where G is the calibration factor, which is determined by measuring a known standard sample in the instrument, assuming that G remains constant for different samples. In turn, the above equation is used to determine the enthalpy of a reaction.
The particle size of the sample influences the DTA results. Generally, both initial and final transition temperatures decrease with decreasing particle size of the sample [8]. This is due to the fact that smaller particle size introduces a larger surface energy to the system. However, contribution of the surface energy is negligible compared with the enthalpy of the reaction for most of the first order phase transitions. In our experiment, we don't need to be concerned about the temperature gradient in the sample since the dimension of Mo-Si-B sample is as small as 3mm.

For accurate measurements, a bulk sample with minimum compositional segregation is preferred, because the DTA data of a bulk specimen is much less affected by oxidation than that of a powder specimen, in that the bulk specimen has much less surface area [9]. In addition, the powder samples may trap air inside and is more difficult to be purged [9]. Powders are also easily blown out of the container during the pumping-down process, which

may cause malfunctioning of the DTA instrument. The Mo-Si-B bulk samples should also be shaped such that it has the best thermal contact with the crucible. A small disk generally fulfills this objective.

The atmosphere can often be varied for various DTA tests. Under static atmosphere conditions, gaseous products cannot be removed rapidly from the vicinity of the sample. This leads to an increase in the partial pressure of the products and the reaction temperature increases. Under dynamic or flowing conditions, evolved gases can be removed from the vicinity of the sample, and the partial pressure of the products remains low [8].

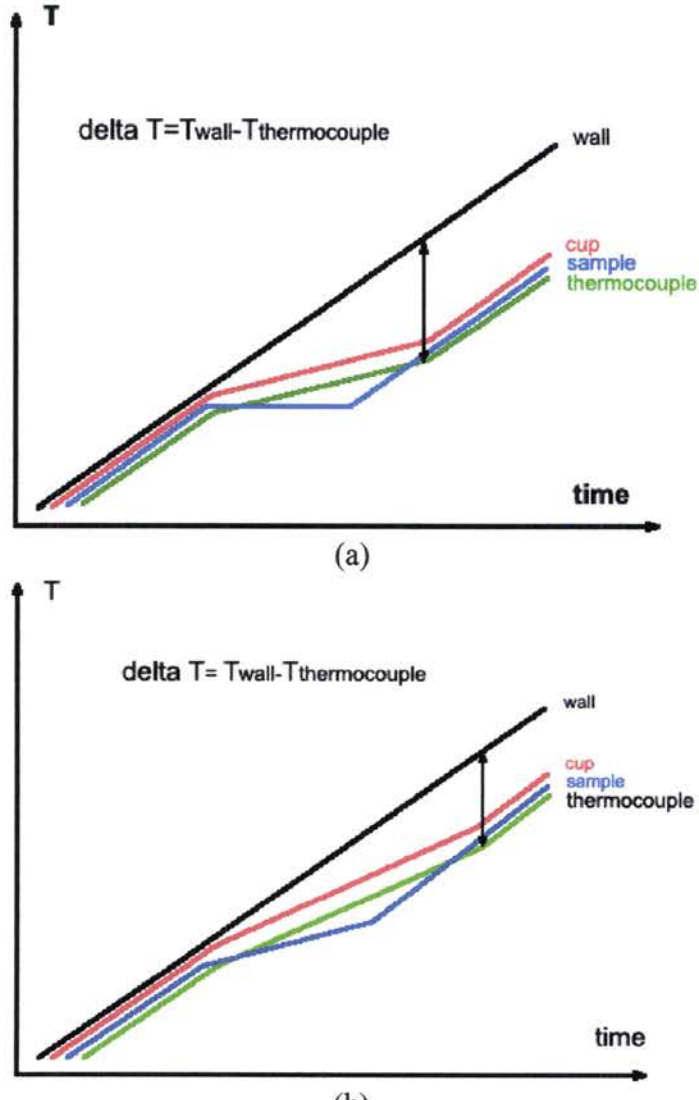

Fig 1.5 Temperature distribution during melting event for (a) pure metal, (b) alloys [30]

It should also be noted that the reaction between the atmosphere and thermocouple, sample holder, gas line or other parts of the apparatus need to be monitored carefully. Some of these issues will be discussed in the preliminary experiments section.

The choice of sample holder, having different shapes and materials, is based on the nature of the sample and experimental conditions. Several factors need to be considered: the reaction between sample holder and sample, the reaction between sample holder and atmosphere, the noise introduced by the holder on DTA/TG signals, the thermal conductivity of the sample holder, etc. [8]

The temperature distribution in the DTA instrument during a melting event is illustrated schematically in Fig 1.5. Pure metals are crystalline materials, so the sample temperature will be held at the melting point during melting until all solid is converted into liquid. Since heat flow exists between the cup and heating element, the cup temperature will continue to increase at a slower rate during melting. And so does the thermocouple temperature. The temperature difference measured is the difference between thermocouple and the wall (heating element). [30]

The situation for alloys is different. The alloy temperature will continue to increase during melting, and so does the cup and thermocouple temperature. From Fig 1.5 we can see that the temperature difference for alloy is smaller for alloys than for pure metals. [30]

DTA instrument measures the temperature difference in terms of voltage difference between sample and reference thermocouples. Practically, the extrapolated onset temperature is considered as the melting point for pure metals. However, it is recommended that the start point of the peak be considered as the melting point for alloys. The peak temperature is usually regarded as the liquidus temperature for alloys.

The maximum temperature gradient between the wall of the sample holder and the center of the sample can be calculated according to the following equations [18]:

For a disk:

$$\gamma_m = \frac{S}{2}\sqrt{\frac{\Delta H \bullet C_p \bullet \varphi}{k}}$$

For a cylinder:

$$\gamma_m = \tau\sqrt{\frac{\Delta H \bullet C_p \bullet \varphi}{2k}}$$

where S is the sample thickness, τ is the diameter of the sample holder, ΔH is the enthalpy of the reaction, C_p is the heat capacity of the sample, ϕ is the heating rate and k is the thermal conductivity [8].

The appearance of TG and DTA curves changes as a result of the difference in packing density. Loosely packed, coarse materials contain space between particles, which reduces the thermal conductivity of the sample [8]. Densely packed samples normally result in a more constant transition temperature with heating rate. To keep the experimental conditions consistent, samples can be melted in the first run and then do a second run to collect data.

Kinetics indicates that whenever possible, a heating curve should be used for determining melting point instead of cooling curve [9]. A very large under cooling is introduced in the solidification process due to nucleation barrier. At least two DTA tests with different heating rate are required to determine a single equilibrium point because of the kinetic effect of heating rate, as mentioned above.

Temperature calibration should be performed on DTA instrument at two temperature points. One temperature to be calibrated should be lower, while the other should be higher than the temperature range of interest. The melting temperature of pure metal is normally used for the purpose of calibration [9]. For the study of metallic system, an empty crucible or a solid piece of pure refractory metal with same mass as reference is recommended. This ensures that the reference material has a stable state, similar thermal mass and heat capacity as the sample to minimize the noise level [25].

Willemin et al [26] studied high temperature phase equilibria in Ni-Al-Ta system. In their work, phase transformation temperatures were determined by monitoring the cooling curve and quenching the specimens at a precise moment. The solid-liquid interface is frozen in rapid cooling and microstructure was studied. [26]

For phase analysis, a specimen was quenched as soon as the first cooling peak is observed; the first solid is already formed and will be situated at the center of the dendrites in the solidified microstructure. Since both the liquidus temperature and the liquid composition

(same as the alloy) were known, analysis of the first-formed solid enabled a tie line to be determined. [26]

For a wide range of compositions, the variations in transformation temperatures were found to be very slight, making it very difficult to determine the extent of the various liquidus regions from the DTA results alone. It was necessary to take into account the microstructural morphology, together with phase analyses and identifications [26].

However, in many alloys the as-cast microstructure was modified by solid-state transformations, so that considerable care was required in interpretation. It showed that the first solid phase formed during solidification could be identified only in the alloy, which was quenched immediately upon reaching the liquidus.

Willemin et al analyzed 85 different compositions and eventually gave a liquidus surface and univariant lines in the Ni-rich region of Ni-Al-Ta system [26]. They identified five primary phase regions namely π, δ, β, γ', and γ, the composition range of these regions as well as the univariant lines in Ni-NiAl-Ni_3Ta triangle.

CHAPTER 2: PRELIMINARY ISSUES OF DTA INSTRUMENT

2.1 Materials compatibility issues

2.1.1 Reaction between Mo-Si-B samples and tungsten crucible

Phase transition temperature, heat of reaction and the reaction rate can be obtained from DTA signal, which is ideal for determining melting or solidification temperatures. Thermogravity (TG) signals give the mass change of sample under controlled temperature program, which indicates change in sample mass at any given temperature [8].

Operating temperature of standard TGA/DTA instruments range from room temperature up to 1500°C. However, measurement for Mo-Si-B requires ultra-high temperature capability up to 2400°C. Working at such high temperature brings a number of issues. Besides the requirement for high temperature capability of the furnace itself, materials compatibility problem for sample and container becomes a serious concern at this temperature regime. Reactions between sample and sample holder, sample and the surrounding atmosphere, the atmosphere and furnace components all have to be taken into consideration when the working temperature rises above 2000°C. Therefore, solving sample containment problem has become a major issue for carrying out characterization in Mo-Si-B experiments.

Fig 2.1 Significant reaction between W and molten T1 + $MoSi_2$ at 2200°C

High melting point and stability make tungsten a qualified material as sample holder in high temperature TGA/DTA devices. The DTA instrument (LINSEIS high temperature DTA/TG, LINSEIS Inc., Germany) uses tungsten as heating element and sample holders. However, molten Mo-Si-B samples turn out to be quite reactive with tungsten at temperatures over 2000°C. Preliminary experiments with Mo-Si-B and tungsten foil showed significant reaction as indicated in Figure 2.1.

According to W-Si binary phase diagram [31], WSi_2 and W_5Si_3 will form from liquid phase at around 2000°C. Since in the DTA experiment Mo-Si-B sample will be melted and have a significant contact area with W sample holder, W-Si or W-Si-B compounds are very like to form.

This type of reaction between the sample and sample holder is not acceptable in that it not only gives incorrect signals but also damages the measuring instrument. Forming metal solid solutions or metal borides is also not allowed for similar reasons. Therefore, it is imperative to find a liner material for the tungsten crucible to contain Mo-Si-B sample.

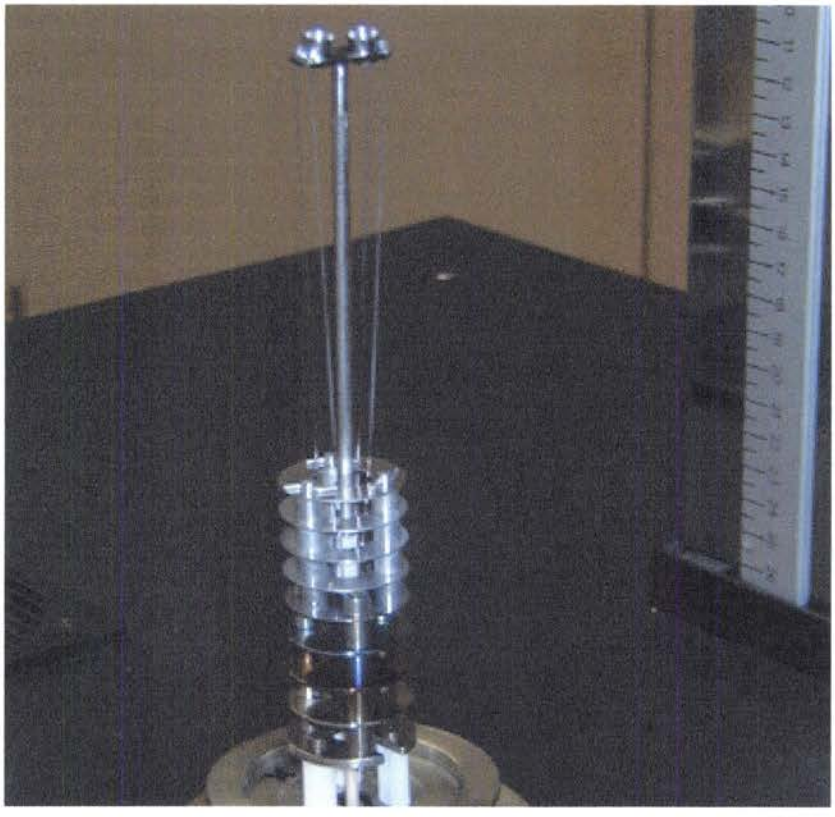

Fig 2.2 Sample holders and shields of DTA instrument

The liner material must meet the following requirements:

(1) It should have a high melting point (>2500°C);

(2) It should not exhibit any destructive phase transformation as sample heated and cooled at relatively high rates;

(3) It should not react with either the sample (metal silicides) or the atmosphere;

(4) It should be processible with reasonable ease and cost.

As shown in Figure 2.2, sample holder assembly of ultra high temperature TGA/DTA unit is quite delicate and the liner needs to fit in the tungsten crucibles provided by the instrument.

After searching around the refractory materials, 8wt% Y_2O_3 stabilized ZrO_2 (YSZ) was found to have a high melting point and a stable state at high temperature regime. Molten YSZ was sprayed on the rounded tips of pre-made graphite rods. The tips of the rods were then cut by a low speed saw (ISOMET, BUEHLER, Lake Bluff, IL) for appropriate crucible size. The crucibles were laid on quartz plates and burnt in a tube furnace (HTF55347P4C 24, LINDEBERG, New Milford, CT) for 48 hours at 1000°C under flowing air. Finally, the crucibles were fired in high temperature furnace (TYPE 46100, THERMOLYNE, Dubuque, IA) at 1400°C in air for 2-3 hours to clean the graphite residuals.

2.1.2 Compatibility of Mo-Si-B and ZrO_2 in carbon-heating-element furnace

In order to protect the instrument from being damaged by unexpected reactions, a series of experiments were first carried out in a carbon-heating-element furnace (ASTRO, Model #1000-2560-FP20, Thermal Technology Inc., Santa Rosa, CA).

A tantalum foil box was employed to wrap the YSZ crucible and the sample in order to prevent the samples and crucibles from being reduced by the carbon atmosphere in the carbon-heating-element furnace. Then the furnace was heated up to 2400°C in both nitrogen atmosphere and in 95 vol% argon and 5 vol% helium (to prevent arcing at high temperature) gas mixture. For the experiment in nitrogen gas, it was obvious that a nitride was formed on the Ta foil and the Ta foil wrap was seriously deformed because of the thermal expansion mismatch between Ta nitride and the pure Ta. This made it impossible to make an airtight Ta

wrap to seal the YSZ crucible and the sample. In the subsequent runs, YSZ crucible was set in graphite felt.

To establish experimental conditions to be used in DTA runs, a number of preliminary experiments were carried out for several combinations of sample, holder and atmosphere. The observations are shown in Table 2.1.

Table 2.1 Materials compatibility tests in carbon-heating element furnace

Sample ID	Description	T (°C)	Atmosphere	Observations
YS2	Mo-Si-B is in YSZ crucible, which is wrapped in Ta box	2400	Ar + He	Ta box was deformed, crucible turned black
YS5	YSZ crucible is mounted in graphite felt	2400	Ar + He	Crucible turned black
YS6	Mo-Si-B in YSZ crucible is mounted in graphite felt	2400	N_2	Crucible turned golden on surface, and became brittle
YS7	YSZ crucible is mounted in graphite felt	2400	N_2	Crucible turned golden on surface, and became brittle

The ZrO_2 crucibles turn black for sample YS2 (with Mo-Si-B in the crucible) and YS5 (without Mo-Si-B), indicating that the blackening of crucibles is caused by the carbon atmosphere rather than the silicides. For samples YS6 and YS7 in N_2 atmosphere, color of both crucibles turned golden, and both crucibles became brittle. This implied that the brittleness of YSZ is due to C + N_2 atmosphere but not from Mo-Si-B because sample YS7 and YS5 differed only in atmosphere. Furthermore, golden coloration was observed only in N_2 atmosphere. Visual observation indicated that there was no chemical reaction between ZrO_2 and Mo-Si-B in either N_2 or Ar + He atmosphere.

BSE (Back Scattered Electron) micrograph of YS2 (Figure 2.3) clearly shows an interdiffusion region between Mo-Si-B and crucible material. The thickness of the

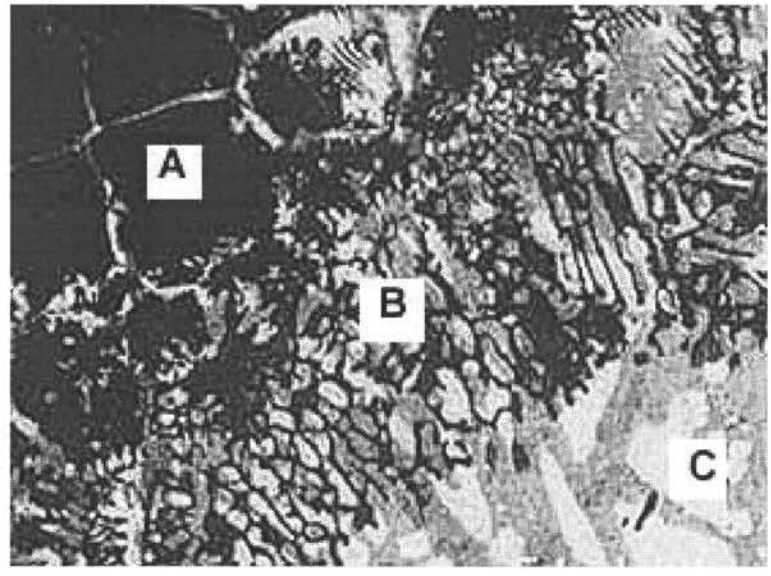

Fig 2.3 BSE micrograph of Mo-Si-B melted in YSZ crucible, argon and helium, 2400°C, 300x. A: ZrO_2; B: interdiffusion region; C: Mo-Si-B

interdiffusion region was less than 0.2mm. A layer of 0.5mm thick ZrO_2 liner would be sufficient to protect tungsten crucible of DTA from the attack of silicide. Further EDS analysis indicates that the dark region on ZrO_2 side (A) shows similar peak intensity for Zr, Mo and Si as the dark region in the interdiffusion region (B). Similarly, peak intensities for Zr, Mo, and Si for the bright region on Mo-Si-B side (C) are comparable to those for the light grains in the interdiffusion region (B). This implies that no measurable chemical reaction occurs between Mo-Si-B and ZrO_2.

2.1.3 Preliminary experiments in DTA apparatus

The containment configuration in DTA apparatus is shown in Fig 2.4. An empty crucible was fired to 2100°C under N_2 atmosphere. The color of crucible turned darker and there was a 0.2% weight loss for the YSZ crucible. This enables us to predict the actual weight change of sample knowing the TG signals.

Mo-Si-B sample contained by YSZ crucible (Fig 2.4) was then melted in nitrogen atmosphere. No signs of reaction between Mo-Si-B and crucible were seen in optical

microscope observations. BSE micrograph (Fig 2.5) of the interface and the EDS spectrum further confirmed this conclusion. The interface between ZrO_2 and Mo-Si-B looked sharp at a magnification of 1000x.

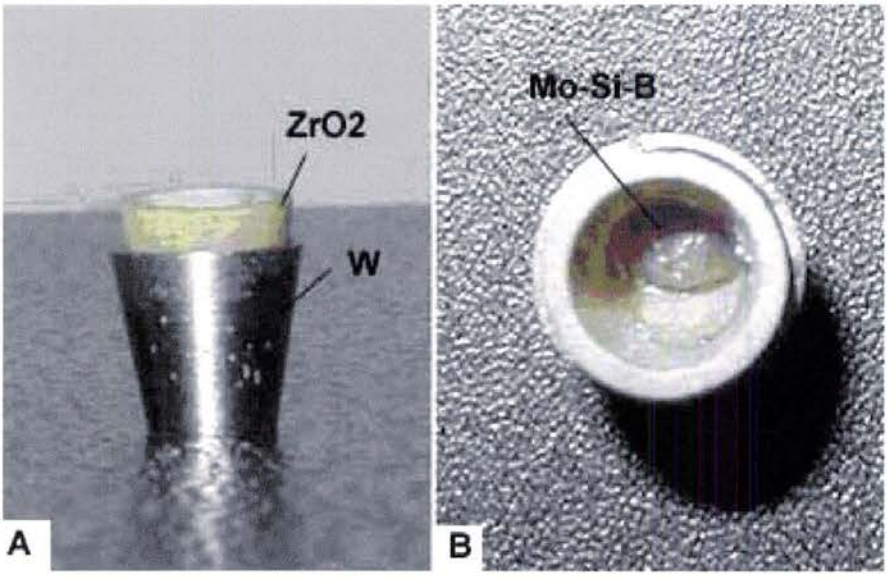

Fig 2.4 Containment configuration for Mo-Si-B in DTA apparatus.
A: side view; B: top view

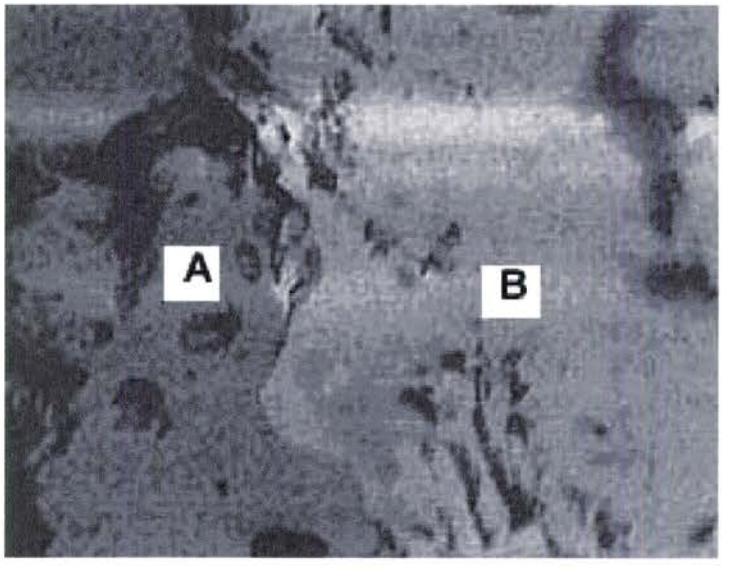

Fig 2.5. BSE micrograph of Mo-Si-B melted in ZrO_2 crucible in DTA, 1000x
A: ZrO_2; B: Mo-Si-B

Another issue is to demonstrate the validity and stability of the DTA signals. A mixture of 60 wt% Al_2O_3 and 40 wt% ZrO_2 powder is used as standard sample in order to eliminate the influence of interdiffusion between ZrO_2 crucible and Al_2O_3 sample. Such sample has a reported eutectic point at 1866±7°C [10] as shown in Fig 2.6.

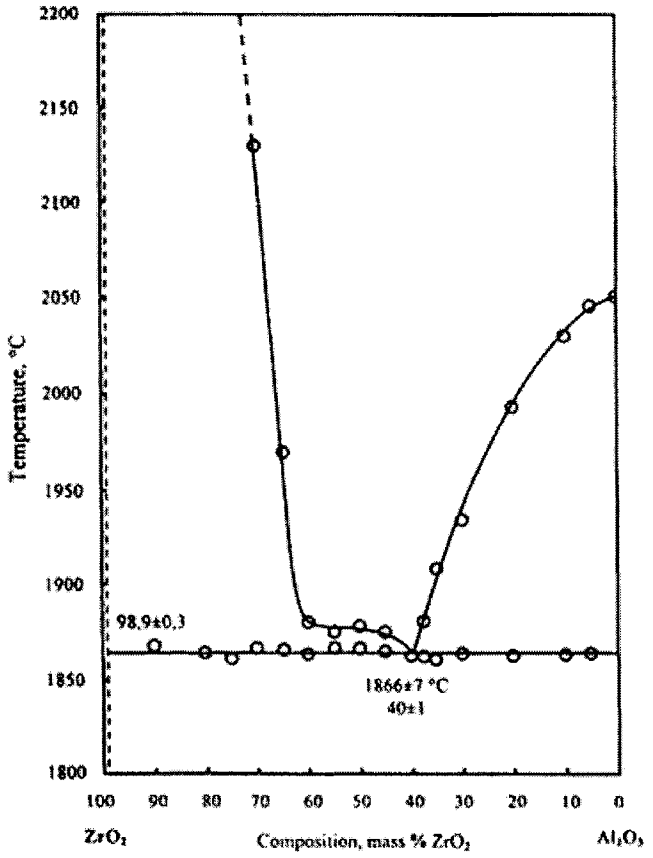

Fig 2.6 Phase diagram of ZrO_2-Al_2O_3 system [10]

The sample was fired in YSZ crucibles as sample holder and reference in nitrogen atmosphere with a heating rate of 10°C/min and then 5°C/min. The DTA curve for 10°C/min heating rate is shown in Fig. 2.7. The software allows measurement, such as temperature and peak area, on the DTA curve. The melting points for the mixture was 1869.6°C and 1863.3°C under heating rate 10°C/min and 5°C/min, respectively. By using the extrapolation method stated above [9], the equilibrium eutectic point is 1837.9°C as shown in Fig 2.8. Assuming a constant thermocouple drift (for this measuring unit at this time, $\Delta T_m(Al_2O_3) = 33°C$), the measured equilibrium eutectic temperature is 1870.9°C, which is within 5-10°C of the literature value. This result demonstrates the validity of the temperature measurement.

The use of YSZ crucible as liner for tungsten sample holder causes a slightly higher noise level. To compensate for that an empty YSZ crucible is used as reference instead of empty tungsten crucible to minimize the noise level. This makes sure that signals from phase transition are identifiable.

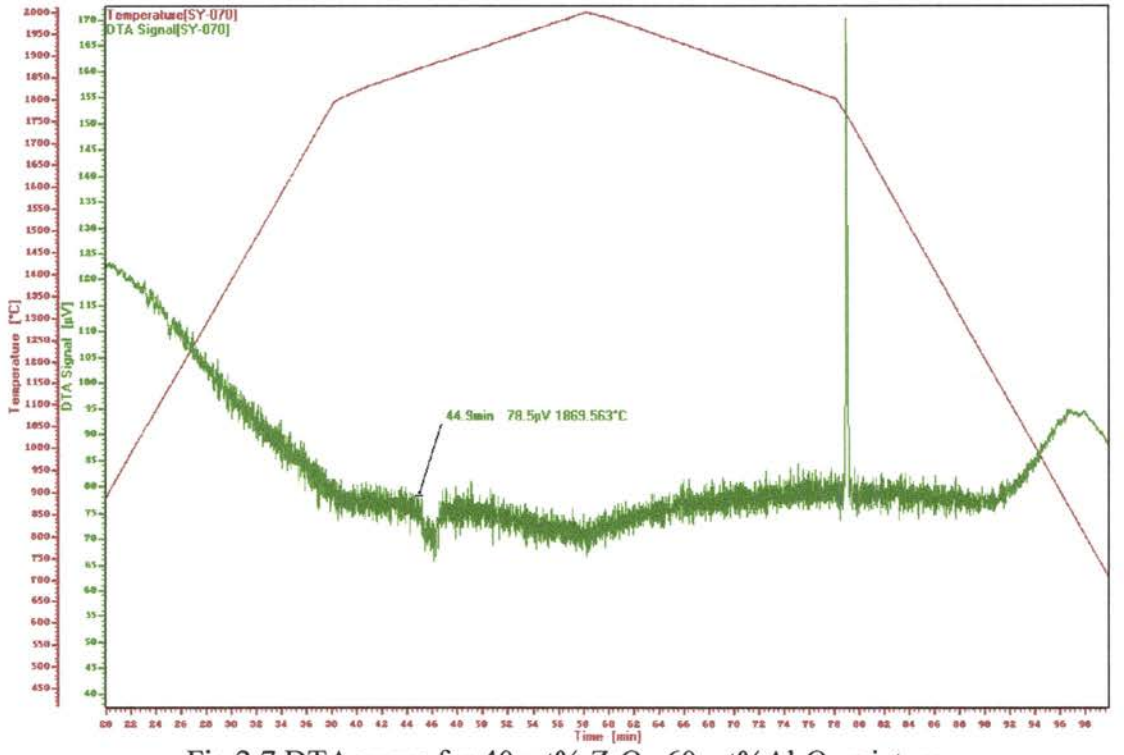

Fig 2.7 DTA curve for 40 wt% ZrO_2-60 wt%Al_2O_3 mixture

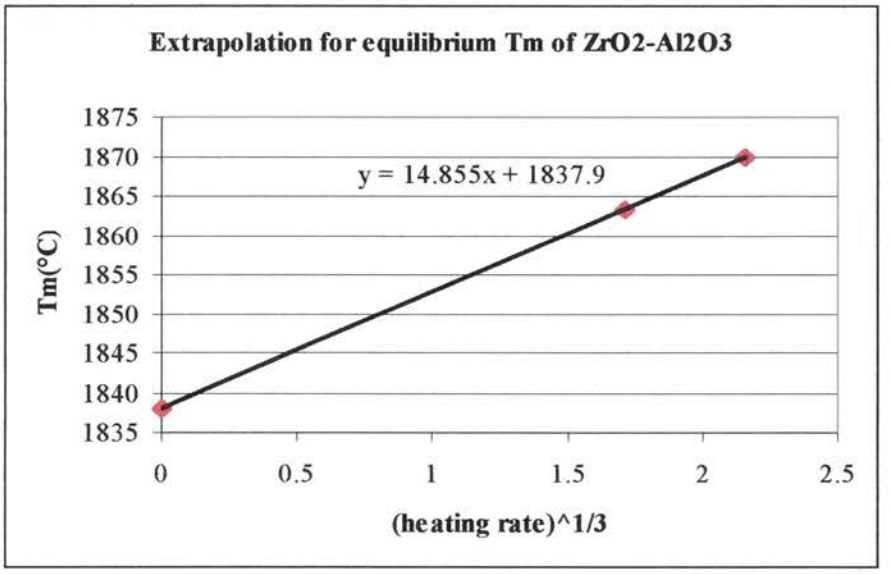

Fig 2.8 Extrapolation for equilibrium melting point of 40wt% ZrO_2 + 60wt% Al_2O_3

2.2 Influence of atmosphere on DTA signals

In order to run a variety of silicides such as Ti-Si-C, argon and helium mixture is considered as the inert atmosphere since nitrogen reacts with the titanium silicide forming titanium nitride. A mixture of 95 vol% argon and 5 vol% helium is used instead of nitrogen. However, the result was not satisfactory even with the standard alumina samples.

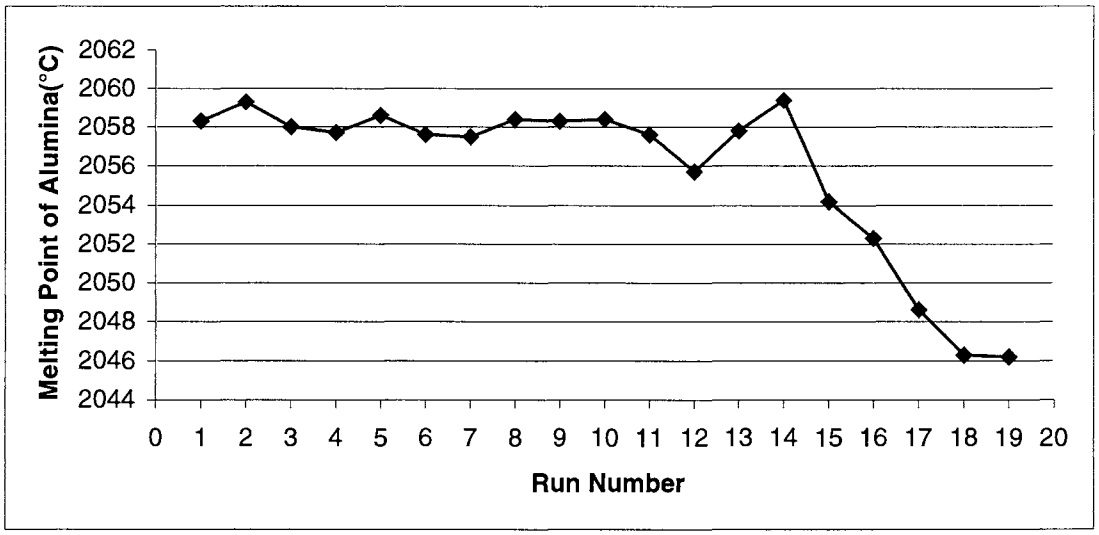

Fig 2.8 Melting temperature of standard alumina sample in different atmospheres
Run number 1~13: N_2; 14~17: 95 vol% Ar and 5 vol% He; 18~19: N_2

Fig 2.8 shows that the melting point of alumina is constant around 2058±2°C from Run #1 to Run #13 with a 25°C/min heating rate in N_2 atmosphere. However, the observed melting point drops precipitously for every run when the atmosphere is switched to argon and helium mixture. The melting point again is stabilized at around 2046°C when atmosphere is switched back to N_2. This brings a limitation of atmosphere that can be used with this instrument. Any sample that reacts with N_2 atmosphere is not suitable because N_2 is needed for maintaining the stability of thermocouples.

Since drift occurs only in Ar + He atmosphere, it must be the cause of the drift. One plausible explanation is that nitrogen helps prevent evaporation of the thermocouples, while argon and helium mixture enables this evaporation. A nitride layer may form on the surface of the thermocouples in nitrogen atmosphere. The type C thermocouples are made of W-5Re alloy and W-26Re alloy. According to the study by Ekstrom et al [29], the nitride layer on tungsten surface leads to the attenuation of the oxygen contamination exponentially:

$$I = I_0 \bullet \exp(-d / \lambda)$$

where λ is the oxygen mean free path (λ=1.55 nm), I_0 (I) is the intensity before (after) nitride layer formation and d is the oxide thickness. Similarly, nitride layer may prevent the evaporation of the alloys, maintaining the stoichiometry of the thermocouples, and therefore, prevent the drift.

2.3 Thermocouple Calibration

Accurate measurement of melting temperature requires calibration of thermocouples and frequent check for their stability.

A number of materials with known melting point were employed as standard for thermocouple calibration. Since most of our DTA runs for Mo-Si-B samples were carried out at 1800-2200°C, standard materials with melting temperatures ranging from 1750-2100°C were selected. Alumina, platinum, and rhodium, along with Mo-22 at% Si, Mo-25.7 at% Si and Mo-34 at% Si compositions were employed for calibration runs. Heating rates ranging from 5°C/min to 25°C/min were used to study the effect of heating rate on the phase transition temperature. All samples except alumina are contained in YSZ crucible. An empty YSZ crucible is used as reference. This containment configuration prevents reaction between silicides and tungsten crucible, while minimizing the signal noise level.. Since alumina forms solid solution with zirconia and has a eutectic reaction with zirconia at around 1866°C, alumina sample was contained in tungsten crucible, with an empty zirconia crucible as reference.

2.3.1 Calibration with alumina, platinum and rhodium

The calibration run results with Al_2O_3, Pt and Rh are summarized in Table 2.2. The extrapolation results for melting temperature versus heating rate are shown in Table 2.3.

The melting temperatures do not have a definite trend with heating rates for any of the three standard materials, which is shown in Appendix II. In fact, the melting temperatures fluctuate randomly within uncertainty of the measurement (±3°C) for heating rate from 5 to 25°C/min. Alumina shows a positive slope and a relatively good linearity for heating rate versus melting temperature plot, while rhodium and platinum show negative slopes. Thus, using either $T - T_0 = C \cdot S$ or $T - T_0 = C \cdot S^{1/3}$ will only introduce larger instability knowing that

the sign of the slope is uncertain. Therefore, neither of the two mathematical models will be used. Instead, the arithmetic average of the measured melting points under 5 to 25°C/min heating rates has a fairly good stability for the three materials. The difference between the reported melting points and the average value of the measurement will be used to correct future measurement.

Table 2.2 Result of DTA runs for Al_2O_3, Pt and Rh under various heating rates

Heating rate S (°C/min)	Al_2O_3	Pt	Rh
5	2030.3	1750.8	1942.2
10	2030.7	1750.1	1941.7
12.3	2030.5	1749.4	1939.9
15	2031.4	1749.8	1940.6
25	2032.6	1749.0	1941.1
10	2028.1	1752.9	1941.9
10	2026.2	1751.0	1940.3
10	2026.7	1748.6	1940.0
10	2026.6	1749.8	1939.5

Table 2.3 Extrapolation for Al_2O_3, Pt and Rh samples

Sample		Al_2O_3	Pt	Rh
$T_{m,\ reported}$ (°C)		2050	1768.4	1964
ΔT_m (°C) for various heating rate		2.3	1.8	2.3
ΔT_m (°C) for 10°C/min		1.9	4.3	2.4
T_0 (°C)	$T-T_0=C\bullet S$	2029.5	1751.3	1941.8
	$T-T_0=C\bullet S^{1/3}$	2026.7	1754.2	1943.5
$T_{m,\ reported}-T_0(S)$ (°C)		20.5	17.1	22.2
$T_{m,\ reported}-T_0(S^{1/3})$ (°C)		23.3	14.2	20.5
$T_{m,\ reported}-\langle T_m\rangle$ (°C)		18.9	18.6	22.9
$T_{m,\ reported}-\langle T_{m(10°C/min)}\rangle$ (°C)		23.1	17.8	23.6

As can be noticed, the measured alumina melting point is different than the previous measurement of around 2058°C. The reason is that two different sets of type-C thermocouples were used for the measurements. The measured temperature values have a strong dependence on the thermocouples, which implies that calibration of thermocouples with standard materials before any measurement is necessary.

We also conclude that the effect of heating rate on the melting temperature for these three materials in this DTA unit is negligible, in that the uncertainty of melting temperature from various heating rate is comparable to the uncertainty from fixed heating rate of 10°C/min. It is suggested that a fixed heating rate of 25°C be used for this DTA unit in the future.

2.3.2 Calibration with molybdenum silicides

In order to better simulate the experimental condition for the Mo-Si-B samples, we use three binary Mo-Si alloys as standard materials for the calibration since the binary Mo-Si phase diagram has been well established. It is obvious that the melting point for sample #2 at 12.3°C/min and for sample #4 at 12.3°C/min are not consistent with other data. Statistically, these two data points can be discarded as they don't belong to the same population.

Table 2.4 Result of DTA runs for Mo-18.8at%Si, Mo-22.2%Si, Mo-27.9at%Si under various heating rates

Heating rate S (°C/min)	#2 (Mo-18.8Si)	#3 (Mo-22.2Si)	#4 (Mo-27.9Si)
5	2000.6	1992.7	1991.8
10	2001.0	1991.6	1992.1
12.3	1996.4	1995.3	1999.6
15	2000.8	1994.4	1991.1
25	2001.2	1991.3	1995.5
10	2002.6	1995.0	N.A.
10	2003.6	1989.8	N.A.
10	2002.9	1990.3	N.A.
10	2003.4	1989.7	N.A.

Table 2.5 Extrapolation for Mo-Si samples

Sample		#2 (Mo-18.8Si)	#3 (Mo-22.2Si)	#4 (Mo-27.9Si)
$T_{m,\ reported}$ (°C)		2025.0	2025.0	2020.0
ΔT_m (°C) for various heating rates		0.6	4.0	4.4
ΔT_m (°C) for 10°C/min		1.0	5.3	N.A.
T_0 (°C)	$T-T_0=C\bullet S$	2000.6	1993.8	1990.0
	$T-T_0=C\bullet S^{1/3}$	1999.9	1994.3	1985.8
$T_{m,\ reported}-T_0(S)$ (°C)		25.7	33.1	30.0
$T_{m,\ reported}-T_0(S^{1/3})$ (°C)		26.0	37.7	34.2
$T_{m,\ reported}-\langle T_m\rangle$ (°C)		25.0	31.9	27.4
$T_{m,\ reported}-\langle T_{m(10°C/min)}\rangle$ (°C)		22.9	33.8	N.A.

The situation for Mo-Si standard materials is similar to alumina, rhodium and platinum. The linearity of melting temperature is poor versus heating rate. The melting temperature varies randomly within the range, shown in Appendix II. Heating rate does not systematically control melting temperature. Therefore, similar action will be taken on the calibration from Mo-Si, which is to take the arithmetic average of the melting points under various heating rates as the measured value. Then the measured value will be subtracted from the reported value to get the correction term.

For the three Mo-Si standard samples, the differences are 25.0°C, 31.9°C and 27.4°C, averaging 28°C. Considering the uncertainty of the measured values under different heating rates, the calibration equation of the thermocouples of the DTA instrument for molybdenum silicides is:

$$T_0 = \langle T_m \rangle + 28 \pm 3°C$$

All measured temperature values after this point are after this calibration.

CHAPTER 3: PHASE TRANSFORMATIONS OF Mo-Si-B AROUND T1 PHASE

The study of liquidus surface of Mo-Si-B system in Mo-rich region is based on the assumption that the position of each phase, the position of the liquidus boundaries, and the position of all the ternary solidification reactions are accurate according to the liquidus projection given by Nunes et al [16], though some of the reported reaction types are questionable.

3.1 Sample preparation

It has been reported by Huebsch et al that samples experience significant weight loss during arc-melting procedure [1]. Therefore, it is not easy to control the composition of the samples if prepared by arc-melting. We adopted an alternative method of sintering mixture of Mo, MoB and T1 powder and annealing at high temperature to reach thermodynamic equilibrium and to minimize the weight loss.

All alloys are prepared from high purity (>99.5%) materials. We use pure Mo metal powders (3-7 micron APS 99.95%, Alfa Aesar, Ward Hill, MA), MoB commercial powders (325 mesh, 99.5%, CERAC, Milwaukee, WI), and single T1 phase powders (>99.5%) from Huebsch's work [1]. Mo, MoB and T1 powders were mixed and ground by mortar and pestle, sieved through a 325-mesh stainless steel sieve and pressed into buttons using a 10mm diameter tungsten carbide lined die at 138MPa.

The buttons are sintered in tungsten heating element furnace in high purity flowing argon for 72 hours at 1780°C. The thermocouples of the furnace are sealed in tubes so that atmosphere does not affect the temperature measurement and control. Sintering was chosen over arc-melting to produce homogeneous and equilibrium phase assemblage. Also Mo, MoB and Mo_5Si_3 powders were chosen over Mo, Si and B powders as starting materials to prevent excessive Si evaporation. The partial pressure of silicon at 1800°C is 0.1atm, while boron and molybdenum are both solid at 1800°C and their partial pressure is 4×10^{-4} atm and 2×10^{-6}atm, respectively. The evaporation rates of Mo, Si, and B are significantly different because of the difference in partial pressure at the sintering temperature. The silicon loss will be most significant, and therefore the stoichiometry of the samples will be changed.

However, Mo, MoB and Mo_5Si_3 all have low vapor pressures at 1800°C, which minimize the change in stoichiometry during sintering.

X-ray diffraction of sample #4 (Mo-27.9Si) shows that the phase assemblages are Mo_3Si and Mo_5Si_3, and no Mo phase is found, while the starting materials are Mo and Mo_5Si_3. Therefore, it is assumed that thermal equilibrium is reached during sintering. Sintered buttons were cut into pellets by diamond saw (Accutom-5, Struers, Cleveland, OH). The pellets were used for DTA, chemical analysis, and X-ray diffraction analysis.

3.2 Chemical analysis of Mo-Si and Mo-Si-B samples

Mo-Si and Mo-Si-B samples were analyzed for silicon and boron contents using ASTM E1097-97 method by Sherry Laboratories (Broken Arrow, OK). The claimed accuracy for the measurement is 1.0at% for silicon and 0.2at% for boron. Five unknown Mo-Si binary samples, two previously analyzed Mo-Si-B samples, and six unknown Mo-Si-B samples were selected for chemical analysis. The nominal composition (starting composition) of these samples and the analyzed contents are shown in Table 3.1 and Table 3.2. The nominal composition for sample #B represents actually the previous chemical analysis from the thesis of Huebsch [1].

Table 3.1 Nominal composition and chemical analysis results of Mo-Si samples

Samples	Nominal composition (at%)		Chemical analysis result (at%)	
	Mo	Si	Mo	Si
#1	90.0	10.0	95.3	4.7
#2	78.0	22.0	81.2	18.8
#3	74.3	25.7	77.8	22.2
#4	66.0	34.0	72.1	27.9
#5	62.5	37.5	80.6	19.4

Table 3.2 Nominal composition and chemical analysis results of Mo-Si-B samples

Samples	Nominal composition (at%)			Chemical analysis result (at%)		
	Mo	Si	B	Mo	Si	B
#B	59.7	38.7	1.6	57.0	41.2	1.8
#B	59.7	38.7	1.6	58.6	39.7	1.7
#10	65.0	28.0	7.0	68.9	26.1	5.0
#11	77.0	13.0	10.0	87.0	9.2	3.8
#12	78.0	20.0	2.0	82.8	17.0	0.2
#13	61.0	29.0	10.0	68.1	22.6	8.3
#15	59.0	22.0	19.0	75.8	10.9	13.3
#16	68.0	24.0	8.0	74.2	20.5	5.3

According to the chemical analysis results for the previously analyzed sample #B, the difference of boron content between the tested value and the known value is 0.1at% - 0.2at%. The repeatability of the tests is also good since the two tests for identical samples (unknown to Sherry Laboratories) differ only 0.1at% in boron content. The content of molybdenum is calculated by difference.

DTA run further confirms the accuracy of the chemical analysis. Mo-Si binary phase diagram [27] indicates a eutectic temperature of 2025°C for Si composition ranging from about 4at% to 25.72at%. But sample #1 (nominal composition Mo-10Si) is not melted in DTA at 2200°C. This implies that the real composition of sample #1 should be in the single Mo phase region. The Chemical analysis result of 4.7 ± 1.0at% Si for sample #1 explains this. Sample #1 may have only 3.7at% of silicon, which makes it in the Mo single-phase region. This may bring the melting temperature of sample #1 over 2200°C.

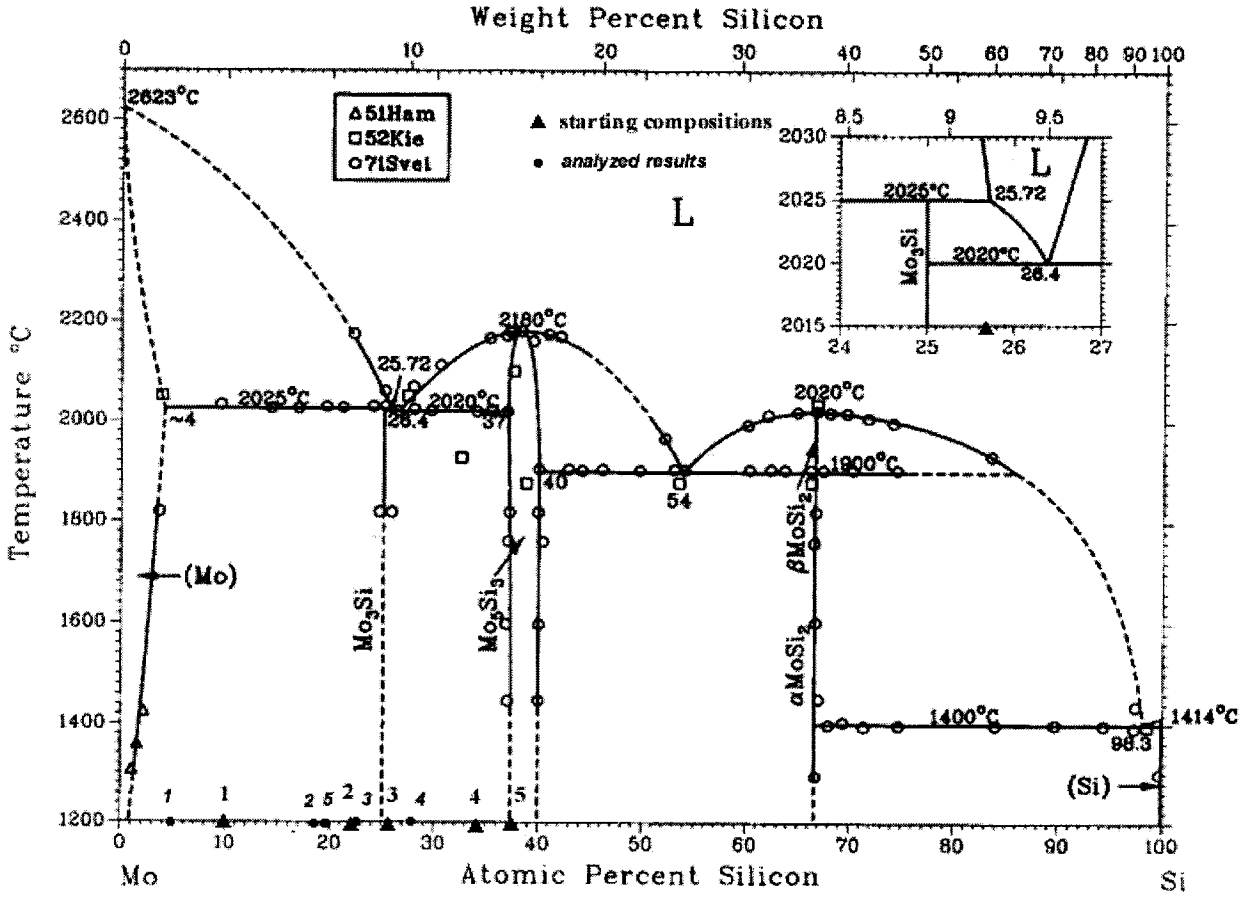

Fig 3.1 Starting sample compositions and chemical analysis results of Mo-Si samples in binary phase diagram [27]

Fig 3.1 shows the starting compositions of Mo-Si samples and the chemical analysis results. The most significant difference between starting and analyzed composition manifests itself for sample #5. Sample #5 changes from $Mo_3Si + Mo_5Si_3$ phase field to that of $Mo + Mo_3Si$. Sample #3 also changes from $Mo_3Si + Mo_5Si_3$ region to $Mo + Mo_3Si$ region. This kind of composition change was also observed by Huebsch [16]. The samples were prepared by first arc-melting Mo, Si and B, and then grinding the arc-melted button and sintering the powders. Their overall sample composition change is less than our result because they lost more Mo during arc-melting, and they lost some Si and B during sintering.

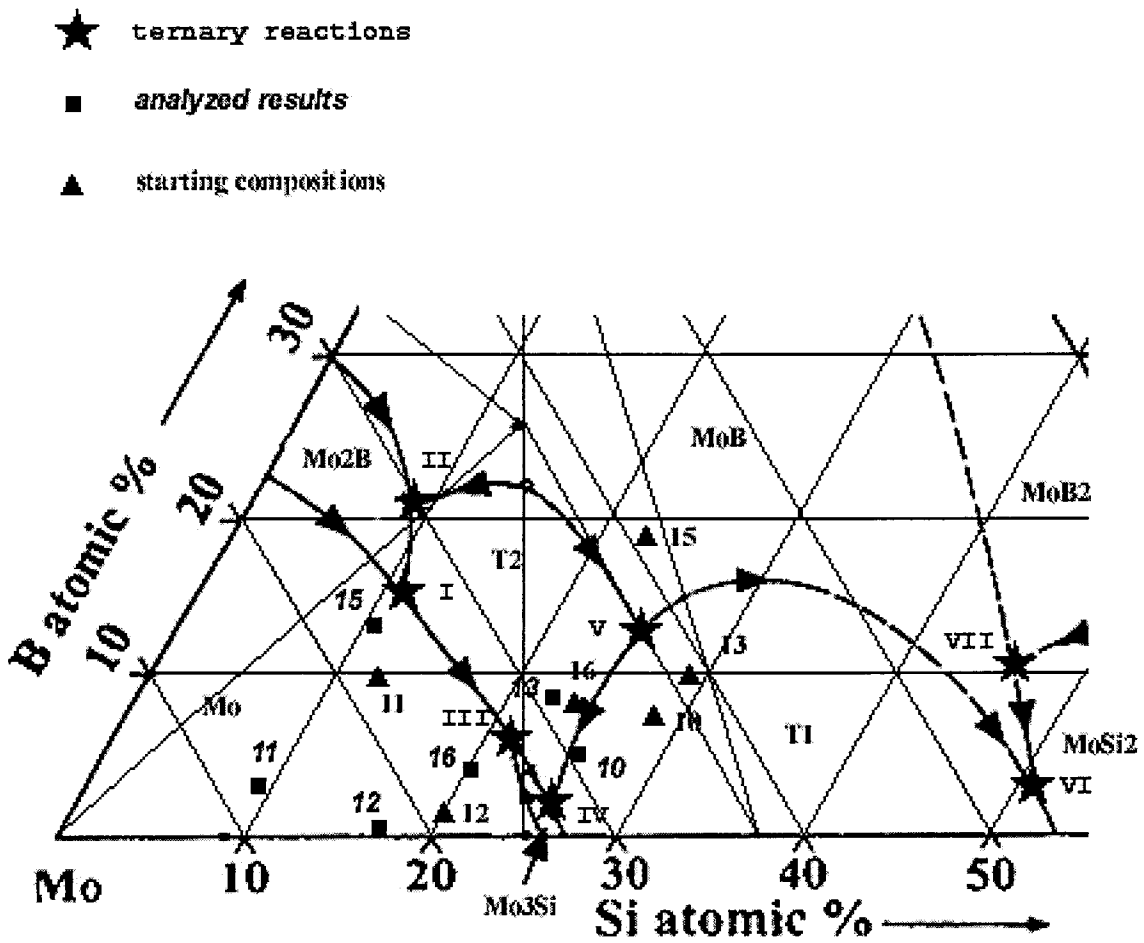

Fig 3.2 Starting sample compositions and chemical analysis results of Mo-Si-B samples in ternary phase diagram [16]

Fig 3.2 shows the starting compositions of Mo-Si-B samples and the chemical analysis results. The most significant shift in the composition was observed for sample #15. It lost 11.1at% of silicon and 5.7at% of boron. Composition of sample #15 moved from MoB primary field across the T2 primary field to Mo primary field. Composition of sample #16 shifted from T2 primary field to Mo primary field. Similarly, sample #13 shifted from T1 primary field to T2 primary field. Sample #10 and #13 are available for studying reaction IV, while sample #11, #12, #15 and #16 should end up at ternary invariant III during their solidification.

Silicon and boron evaporation occurs for all the sintered Mo-Si and Mo-Si-B samples. The Mo-Si-B samples usually lose up to 10at% of silicon and up to 7at% of boron. Therefore, the stoichiometry and even the phase assemblage of the samples are changed, and

hence, chemical analysis is necessary to determine the true composition of the sintered samples. According to the above discussion for sample #1 and sample #B, it is safe to assume that the accuracy of chemical analysis for Si is 2.0at% and for B is 0.5at%. So the accuracy for Mo is 2.5at%. On the other hand, it is very difficult to prepare equilibrium condition Mo-Si-B samples with good composition control because the weight loss of silicon and boron is inevitable and cannot be controlled easily. We need to start from higher silicon and boron content in order to have the designated compositions with extended sintering process.

3.3 Determination for the nature of reaction IV

If we draw the Alkemade lines (Fig 3.2) between these solid phases, we can see that reaction IV is in the Alkemade triangle of T2-Mo_3Si-T1. The primary solid phase regions around IV are also T2, Mo_3Si and T1. According to phase rule, reaction IV should be ternary eutectic: $L \rightarrow T1 + T2 + Mo_3Si$. Furthermore, the Alkemade line T2-Mo_3Si intersects with the liquidus boundary between T2 and Mo_3Si. The intersection should be a high temperature point on the boundary curve, which also indicates that reaction IV should be eutectic. However, Nunes et al [16] claimed that reaction IV is a peritectic reaction: $L + T1 \rightarrow T2 + Mo_3Si$ [16]. The nature of this reaction needs to be re-examined.

The microstructure of the as-cast sample #13 is shown in Fig 3.3. Since boron is a light element which cannot be detected with back-scattered electron detector, the brightness of the phases depends on the Mo:Si ratio. Therefore, T2 phase has the highest brightness, then Mo_3Si, and T1 phase is the darkest.

T2 phase solidify first and has a relatively longer time for growth, which results in the brightest areas in Fig 3.3(a). After the liquid composition reaches the liquidus boundary between T2 and T1, binary eutectic reaction is observed and T1 and T2 phases solidify simultaneously. A slightly darker phase forms around the bright T2 phase in Fig 3.3(b). this must be Mo_3Si phase.

At higher magnification (5000x), an even darker phase is evident as finely dispersed in this phase. EDS analysis on these brighter and darker spots indicated that the composition is close to those relatively large dark (T1) and bright (T2) regions in Fig 3.3 (b), which indicates fine ternary eutectic structures. Based on the sample composition, the ternary eutectic reaction yields:

$$L \rightarrow 0.9130 \bullet Mo_3Si + 0.0435 \bullet Mo_5Si_3 + 0.0435 \bullet Mo_5SiB_2$$

So the ternary eutectic structure is mostly Mo_3Si phase, with small amount of T1 and T2, which is consistent with the observation from BSE image. No peritectic structure has been observed. Therefore, we conclude that reaction IV is a ternary eutectic reaction.

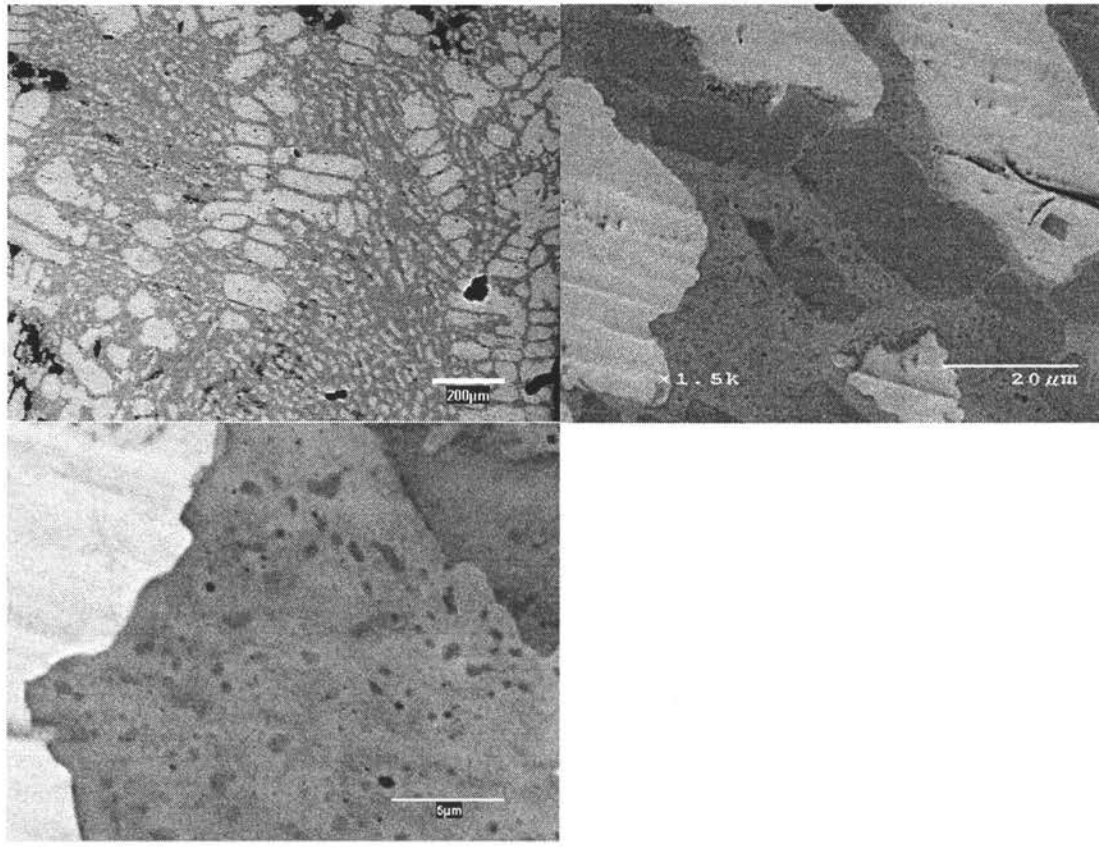

Fig 3.3 BSE micrograph of as-cast sample #13.

(a) 80x, the bright islands are T2 phase; darker areas are the rest phases.

(b) 1500x, the darkest areas are Mo_3Si, brightest areas are T2, and less dark areas are the rest phases.

(c) 5000x, in the middle region, small amount of T1 and T2 phases disperse in the majority of Mo_3Si phase.

3.4 DTA tests of Mo-Si-B samples

3.4.1 DTA test results

DTA tests were performed using ultrahigh temperature commercial DTA instrument. All samples were contained in a tungsten crucible with yttria stabilized ZrO_2 (YSZ) liner. Holder for reference was empty crucible. All tests were performed at a fixed heating and cooling rate of 25°C/min during the process of melting and solidification. The nitrogen flow rate was 50ml/min.

Table 3.3 DTA test results for as-cast Mo-Si-B samples

Sample # Composition	T_{onset} (°C) of 1st peak	Other peaks	Solidification peaks
#10 68.9Mo-26.1Si-5.0B	1936	None	1 small, then 1 large
#11 87.0Mo-9.2Si-3.8B	1922	None	2 large
#12 82.8Mo-17.0Si-0.2B	1926	Second peak is largest, onset 1989°C, no other peaks	1 large, then 1 small
#13 68.1Mo-22.6Si-8.3B	1940	None	2 large
#15 75.8Mo-10.9Si-13.3B	1923	Second peak onset 1965°C	2 large, then 1 small
#16 74.2Mo-20.5Si-5.3B	1923	None	1 small, then 1 large

Sintered Mo-Si-B samples were cut to small solid pieces with weight around 80mg. Each sample was heated up to 2300°C and cooled down to room temperature. Two consecutive runs were recorded for each sample. Therefore, samples in the first run are considered as-sintered condition, while the samples in the second run are as-cast condition. Table 3.3 shows the DTA test results on the as-cast condition Mo-Si-B samples. The DTA results of the as-sintered samples are similar to the as-cast samples except that the former

exhibit additional noise signals. Therefore, the as-cast samples DTA curves are used for peak area calculation.

The first melting event represents the ternary eutectic reaction. Sample #10 and #13 starts with congruent melting IV, while sample #11, #12, #15, #16 with III. The reaction temperature of III and IV can be calculated by taking the arithmetic average of the onset points of the first peaks from Table 3.3. Therefore,

$T_{III} = 1924 \pm 3°C$

$T_{IV} = 1938 \pm 3°C$

3.4.2 Melting and solidification of the Mo-Si-B samples

As for melting, it is the reverse process of solidification. However, the difference is that solidification completes in a very short time and has a large under-cooling. It is impractical to use the temperature measured from solidification to determine the phase transformation temperature. But we still can tell the number of solidification reactions from the number of solidification peaks. Melting is a continuous process for Mo-Si-B samples. Usually ternary congruent or incongruent melting occurs first, followed by a binary congruent melting and at last, a single phase melting. There is no distinct boundary on the DTA heating curve between these consecutive melting events. The DTA signal for melting is normally a broad peak or set of peaks. We consider the onset point of the first peak as the ternary melting temperature.

Sample #11, #12, #15 and #16 are in the Alkemade triangle of Mo-T2-Mo_3Si, so the room temperature as-cast phase assemblages should be Mo, T2 and Mo_3Si. Sample #10 and #13 have room temperature phase assemblages of Mo_3Si, T1 and T2 for similar reason. According to the phase diagram shown in Fig 3.2, the fraction of each phase in the samples can be determined by the lever rule. The results are shown in Table 3.4.

Table 3.4 As-cast sample phase assemblages

Phases	Mo (mol%)	Mo_3Si (mol%)	Mo_5SiB_2 (mol%)
#11	85.8	11.3	2.9
#12	65.0	34.8	0.2
#15	73.2	10.4	16.4
#16	26.5	64.0	9.5
Phases	**Mo_3Si (mol%)**	**Mo_5SiB_2 (mol%)**	**Mo_5Si_3 (mol%)**
#10	67.7	13.2	19.1
#13	61.8	25.7	12.5

*Based on chemical analysis results, the accuracy is 1.0mol%.

Sample #13 is hereby illustrated for the solidification path as an example. Other samples have similar solidification process.

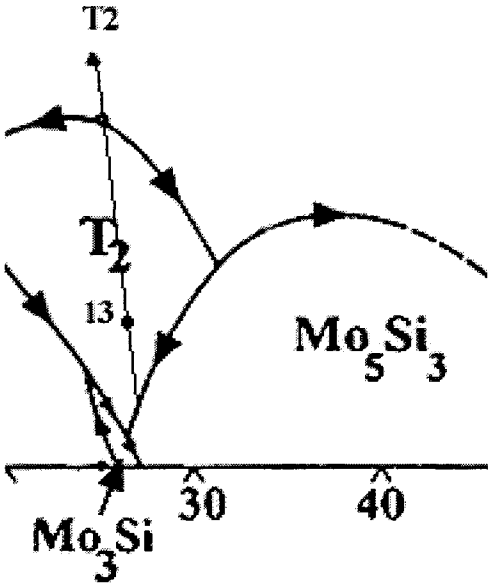

Fig 3.4 Illustration for solidification path of sample #13

As sample #13 is cooled from liquid, the first solid to appear is T2 and the liquid composition move along the extension of tie line T2-13 toward the liquidus boundary between Mo_5Si_3 and T2 (Fig 3.4). The first peak on the DTA solidification curve indicates the heat released in this process.

Binary eutectic reaction L +T2 → L + T1 + T2 starts after the liquid composition reaches the T1, T2 boundary. Since distance between the intersection of T2-13 and T1, T2 boundary is fairly short, the liquid composition doesn't change much before it reaches the ternary eutectic point, which implies only small amount of T1 + T2 is formed. Normally, the temperature range from the start of first solid to the end of last solid for each solidification reaction is about 5°C. Therefore, this binary eutectic reaction releases small amount of heat, which is not sufficient to give an identifiable peak on the DTA curve.

At ternary eutectic point, reaction L + T1 + T2 → T1 + T2 + Mo_3Si occurs until all liquid solidifies. This reaction releases relatively large amount of heat and gives a large solidification peak on the DTA signal. The eutectic temperature for reaction IV is indicated from the onset point of the first peak, which is 1940°C.

Sample #10 is in Alkemade triangle Mo_3Si-T1-T2, so it experiences solidification reactions: L → T1, L + T1 → T1 + T2, and L + T1 +T2 → Mo_3Si + T1 +T2. Sample #11 and #15 are in the Alkemade triangle of Mo-T2-Mo_3Si, so they all end with ternary eutectic reaction L + Mo + T2 → Mo + T2 + Mo_3Si. Sample #12 and #16 are also in triangle Mo-T2-Mo_3Si, however their binary eutectic reaction, L + Mo → Mo + Mo_3Si, differs from that of #11 and #15. Therefore, the ternary eutectic reaction for sample #12 and #16 is L + Mo + Mo_3Si → Mo + Mo_3Si + T2, which is also different from that of #11 and #15.

3.4.3 Calculation of the reaction heat for reaction III and IV

The peaks of the DTA signals are caused by the temperature difference between the sample and the reference, which results from the sample reaction heat change. For the DTA instrument, the heat change of the reaction ΔH (J/kg) is proportional to the peak area, ΔA(μ Vs/mg).

We assume that the proportionality constant k between ΔH and ΔA is constant for all samples under same heating rate and the same gas flowing rate. Rhodium is used as standard sample to measure k. The heating rate is constant at 25°C during all phase transformations for all samples including Rhodium, and the nitrogen flowing rate is kept constant at 50ml/min.

ΔA_{Rh}=6.52 μ Vs/mg, ΔH_{Rh}=21.76 kJ/mol=2.11×10^5 J/kg

$$k = \frac{\Delta H_{Rh}}{\Delta A} = 3.24\times10^4 C/s$$

Sample #15 and #16 were used to calculate the heat exchange for reaction III: L → Mo + T2 + Mo_3Si. Heat exchange for reaction IV: L → T1 + T2 + Mo_3Si was calculated from sample #10 and #13.

Sample #15 is hereby taken as an example to show the calculation for the reaction heat.

The peak area measured from the first endothermal peak is $\Delta A=4.25\ \mu$ Vs/mg for sample #15. The mass of the sample is measured before the DTA test. The reaction heat for III is:

$$\Delta H_{reactionIII} = k \bullet \Delta A / C$$

C represents the mass fraction of sample #15 involved in reaction III.

Assume 1 mol of product is generated from reaction III. The position of reaction III in the ternary phase diagram is 73at%Mo-21at%Si-6at%B. Therefore, the exact ternary eutectic reaction according to the lever rule is:

$$L \rightarrow 0.16 \bullet Mo + 0.72 \bullet Mo_3Si + 0.12 \bullet Mo_5SiB_2$$

Assume 1mol of as-cast condition sample #15 is in the DTA test. There are three melting reactions:

$$L \rightarrow Mo + Mo_3Si + Mo_5SiB_2$$
$$L \rightarrow Mo + Mo_5SiB_2$$
$$L \rightarrow Mo$$

All the Mo_3Si is generated in the ternary eutectic reaction. According to Table 5.5, there are 0.104 mol Mo_3Si, 0.732 mol Mo, 0.164 mol T2 and the mass for each phase is 32.86g, 70.23g and 86.82g, respectively. The entire sample mass is 189.91g.

According to the portion of the three phases in reaction III,

$$\frac{Mo}{0.16} = \frac{Mo_3Si}{0.72} = \frac{T2}{0.12}$$

The amount of each phase in the reaction is: Mo: 0.023mol, 2.21g; Mo_3Si: 0.104mol, 32.86g; Mo_5SiB_2: 0.017mol, 9.00g. Total mass in the reaction is 44.07g. The mass fraction of sample #15 included in reaction III is:

$$C = \frac{44.07}{189.90} = 0.232$$

Therefore, the reaction heat for III is:

$$\Delta H_{reactionIII} = k \bullet \Delta A / C = 5.95 \times 10^5\ J/kg$$

Similarly, the reaction heat for III calculated from sample #16 is $5.83 \times 10^5\ J/kg$. Reaction heat for IV calculated from sample #10 and #13 are $8.85 \times 10^5\ J/kg$ and

$9.12\times10^{5}\ J/kg$, respectively. The uncertainty is about 10% of the absolute value. The average reaction heat for III and IV are:

$$\Delta H_{reactionIII} = 5.89 \pm 0.06\times10^{5}\ J/kg$$

$$\Delta H_{reactionIV} = 8.99 \pm 0.09\times10^{5}\ J/kg$$

CHAPTER 4: CONCLUSIONS

In this investigation, a process for carrying out ultrahigh temperature DTA tests for Mo-Si-B intermetallics was developed to study the phase transformation for compositions around T1 phase. Containment of the Mo-Si-B samples in the tungsten sample holder issue was solved by using yttria-stabilized zirconia crucibles. Linear and cubic root model for interpreting the relationship between phase transformation temperature and heating rate were discussed. Within the experimental conditions studied, linear and cubic root models did not result any better extrapolated temperatures than the simple arithmetic average.

The effect of gas atmosphere on the DTA instrument, the testing results and the samples were discussed. Nitrogen turned out to be the only plausible inert atmosphere for ultrahigh temperature DTA experiments for Mo-Si-B samples. Argon and helium mixture degraded the type C thermocouples and caused drift of measured temperature. Optimum gas flow rate is also determined to be 50 ml/min.

Calibration work on the W-Re thermocouples of the DTA instrument was carried out from 1700°C to 2100°C. Alumina, rhodium, platinum as well as known molybdenum silicides were adopted as standard materials for the calibration. Finally, equation T0 = Tm + 28 ±3°C was adopted to interpret the equilibrium melting temperature from measured values for Mo-Si-B materials.

All Mo-Si-B samples were prepared from high purity (>99.5%) Mo, MoB and Mo5Si3 powders. All samples were annealed at 1780°C for 72 hours to reach equilibrium. Equilibrium phase assemblages were verified by X-ray diffraction analysis. However, chemical analysis indicates that the composition of samples drifted significantly from the starting composition, as a result of evaporation of silicon and boron during sintering or annealing. A relatively shorter annealing time is suggested for future work.

The study for liquidus surface of Mo-Si-B system on Mo-rich region is based on the liquidus projection by Nunes et al [16]. It was assumed that all the liquidus boundaries and reaction positions in the phase diagram from their study were accurate. This study was focused on two ternary solidification reactions, III: L → Mo + T2 + Mo3Si, and IV: L → T1 + T2 + Mo3Si. The nature of reaction IV was clarified to be a eutectic reaction rather than

peritectic as claimed by Nunes et al [16] by studying the microstructure. The solidification paths for all the Mo-Si-B samples were studied. Temperatures for reaction III and IV were found to be 1924±3°C and 1938±3°C, respectively. It was assumed that the reaction heat was proportional to the peak area of the DTA signals. The reaction heat for III and IV is calculated from DTA measurement to be: $\Delta H_{reactionIII} = 5.95\times10^5$ J/kg and $\Delta H_{reactionIV} = 8.99\times10^5$ J/kg, respectively.

This research demonstrated that ultra high DTA can be used effectively for determining melting temperature for very high melting compounds or phases provided experimental conditions are carefully controlled including sample reactions with crucible, atmosphere as well as reaction of the latter with the components of the instrument.

REFERENCES

1. J.J. Huebsch, MS Thesis, Iowa State University, Ames, Iowa, 1998.
2. K. Kurokawa, H. Houzumi, I. Saeki, H. Takahashi, "Low temperature oxidation of fully dense and porous $MoSi_2$," Materials Science and Engineering A, **261**, no. 1-2, 292-299, Mar. 15, 1999.
3. S. K. Ramasesha, K. Shobu, "Oxidation of $MoSi_2$ and $MoSi_2$-based materials," Bulletin of Materials Science, **22**, No. 4, 769-773, Jun., 1999.
4. M.K. Meyer, M. Akinc, "Oxidation behavior of boron-modified Mo_5Si_3 at 800°C-1300°C," J. Am. Ceram. Soc., **79**, No.4, 938-44, 1996.
5. R.W. Bartlett, J.W. McCamont, and P.R. Gage, "Structure and chemistry of oxide films thermally grown on molybdenum silicides," J. Am. Ceram. Soc., **48**, No.11, 551-58, 1965.
6. M.K. Meyer, A.J. Thom, and M. Akinc, "Boron-doped molybdenum silicides for structural applications," Intermetallics, **7**, 153-162, 1999.
7. H. Nowotny, E. Dimakopoulou, H. Kudielka, "Undersuchrngen in den driestoffsystemen: molybdan-silizium-bor, wolfram-silizium-bor und in dem systen: VSi_2-$TaSi_2$," Mh Chem., **2**:180-189, 1957.
8. T. Hatakeyama, Zhenhai Liu, Handbook of Thermal Analysis, John Wiley & Sons, London, New York, 40-45, 1998.
9. Y.T. Zhu, J.H. Devletian, A. Manthiram, "Application of differential thermal analysis to solid-solid transitions in phase diagram determination," J. Phase Equilibria, **15**, No. 1, 37-41, Feb, 1994.
10. D.A. Jerebtsov, G.G. Mikhailov, and S.V. Sverdina, "Phase diagram of the system: Al_2O_3-ZrO_2,"Ceramics International, **26**, 821-823, 2000.
11. K. Yanagihara, T. Maruyama, and K. Nagata, "The intermediate and high temperature oxidation behavior of $Mo(Si_{1-x}Al_x)_2$ intermetallic alloys," Intermet., **3**, 243-51, 1995.
12. J.H. Schneibel, C.T. Liu, D.S. Easton, and C.A. Carmichael, "Microstructure and mechanical properties of Mo-Mo_3Si-Mo_5SiB_2," Materials Science and Engineering, **A 261**, 78-83, 1999

13. J.H. Schneibel, C.T. Liu, L. Heatherly, Jr., and C.A. Carmichael, "Processing and properties of molybdenum silicide intermetallics containing boron," Annual Conference on Fossil Energy Materials, Knoxville, TN, May 20-22, 1997.
14. J.J. Huebsch, M.J. Kramer, H.L. Zhao, and M. Akinc, "Solubility of boron in $Mo_{5+y}Si_{5-y}$," Intermetallics **8**, 143-150, 2000.
15. M. Akinc, M.K. Meyer, M.J. Kramer, A.J. Thom, J.J. Huebsch, and B. Cook, "Boron-doped molybdenum silicides for structural applications," Materials Science and Engineering, **A 261**, 16-23, 1999.
16. C.A. Nunes, R. Sakidja and J.H. Perepezko, "Phase stability in high temperature Mo-rich Mo-B-Si Alloys", Structural Intermetallics, 831-839,1997.
17. S. Speil, L.H. Berkelhamer, J.A. Pask, and B. Davis, US Bur. Mines Tech. Pap., 664, 1945.
18. R. D. Weir, "Thermophysics of advanced engineering materials," Pure Appl. Chem., **71,** No. 7, 1215-1226, 1999.
19. P.A.G. O'Hare, "Thermochemistry of silicon-containing materials," Pure Appl. Chem., **71**, No. 7, 1243-1248, 1999.
20. X. Fan, K. Hack, T. Ishigaki, "Calculated C-$MoSi_2$ and B-Mo_5Si_3 pseudo-binary phase diagrams for the use in advanced materials processing," Materials Science and Engineering, **A 278**, 46-53, 2000.
21. D. R. Lide, Handbook of Chemistry and Physics, 82nd edition, 5-4 – 5-23, 2001-2002.
22. Periodic table of elements, Johnson Matthey, 1989.
23. F. Cardarelli, Materials Handbook: a concise desktop reference, Springer, London, Berlin, Heidelberg, New York, Barcelona, Hong Kong, Milan, Paris, Singapore, Tokyo, 337-369 , 2000.
24. M.E. Brown, Introduction to Thermal Analysis, Chapman and Hall, London, 41-231, 1988.
25. R. D. Shull, "Application of thermal analysis techniques to phase diagram determinations," Thermal Analysis in Metallurgy, edited by R. D. Shull and A. Joshi, The Minerals, Metals & Materials Society, 95-119,1992.

26. P. Willemin, O. Dugue, M. Durand-Charre, J. Davidson, "High temperature phase equilibria in the Ni-Al-Ta system," The Metallurgical Society/AIME, 637-647, 1984.
27. A.B. Gokhale and G.J. Abbaschian, "The Mo-Si (Molybdenum-Silicon) System," J. Phase Equilibria, **12**, No. 4, 493-498, Aug, 1991.
28. Eric M. Summers, MS Thesis, 88-97, Iowa State University, Ames, Iowa 1999.
29. B.M. Ekstrom, S. Lee, N. Magtoto, J.A. Kelber, "Cu wetting and interfacial stability on clean and nitrided tungsten surfaces," Applied Surface Science **171**, 275-282, 2001.
30. Bill Boettinger, Presentation at Ames Laboratories, April, Ames Iowa, 2002.
31. HTTP://www.met.kth.se/pd/, May 10, 2002.

ACKNOWLEDGEMENTS

Ames Laboratory is operated for the US Department of Energy by Iowa State University under contract number W-7405-ENG-82. This research was supported by the Office of Basic Energy Science, Materials Science Division.

Special thanks to my parents for their support and encouragement. I would also like to thank Dr. Andrew Thom for his assistance throughout this work, and Matthew Besser for providing zirconia crucibles. I would like to thank my colleagues Chuanping Li, Xiang Wei and Heath Reimers for their help.

This work could not be completed without the instruction and criticisms from my major professor Dr. Mufit Akinc. His contribution to this work is greatly appreciated.

Finally, thanks to my graduate committee, Dr. Mufit Akinc, Dr. Matthew Kramer and Dr. Gordon Miller.

APPENDIX I: DTA CURVES OF AS-CAST Mo-Si-B SAMPLES

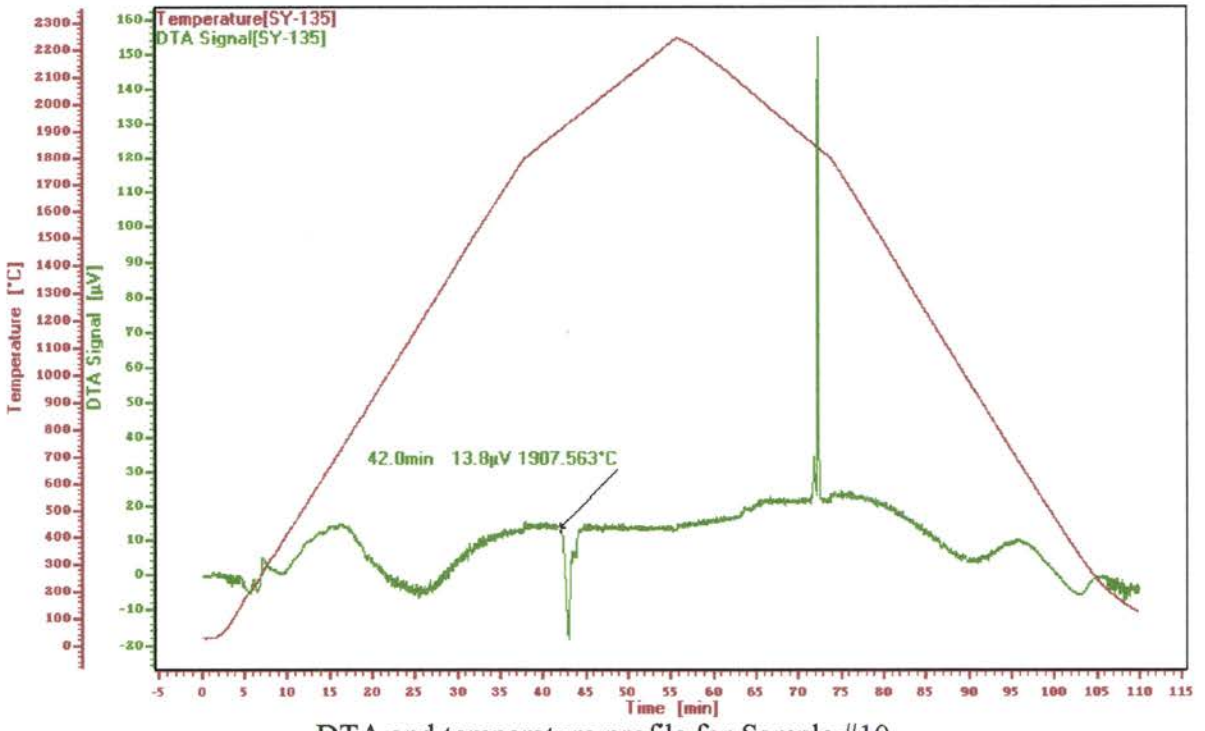

DTA and temperature profile for Sample #10

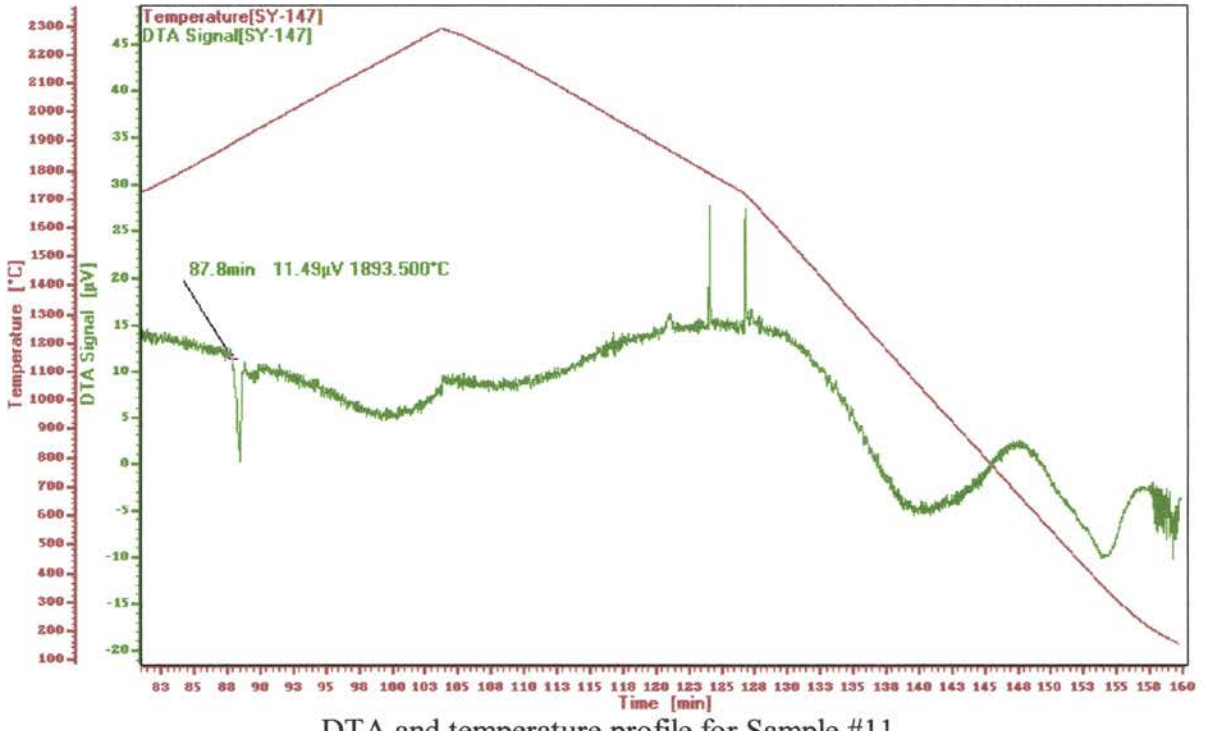

DTA and temperature profile for Sample #11

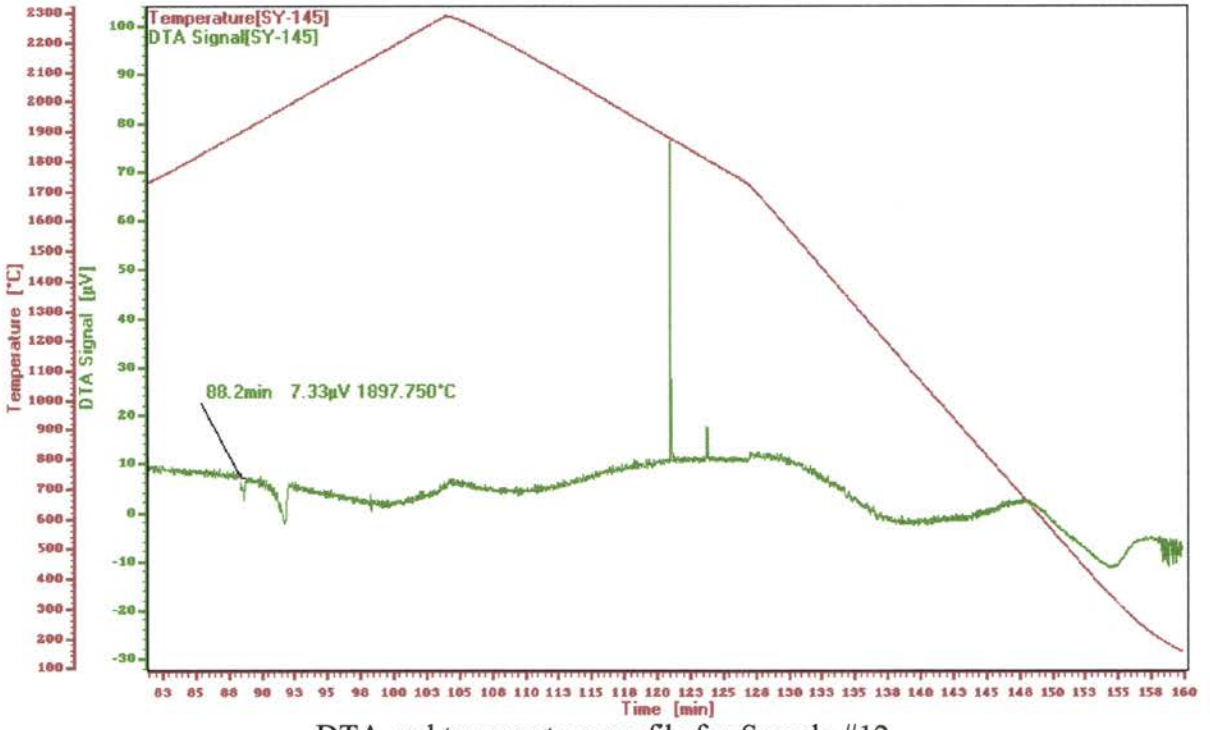

DTA and temperature profile for Sample #12

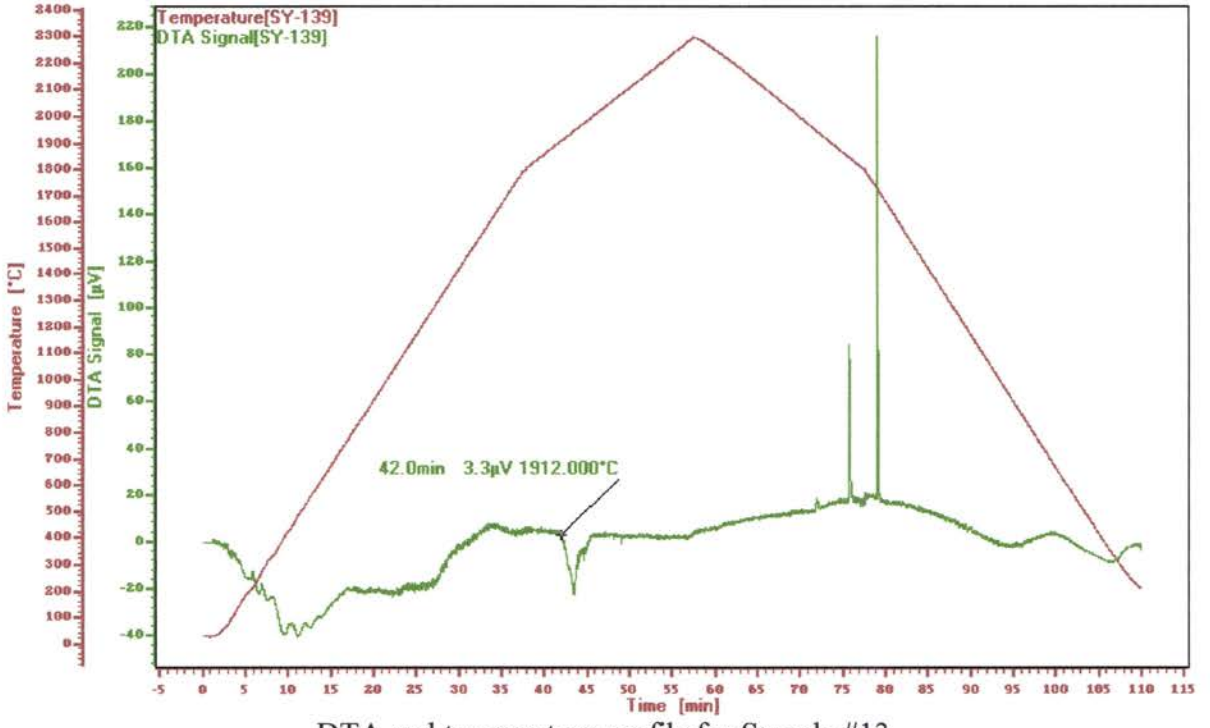

DTA and temperature profile for Sample #13

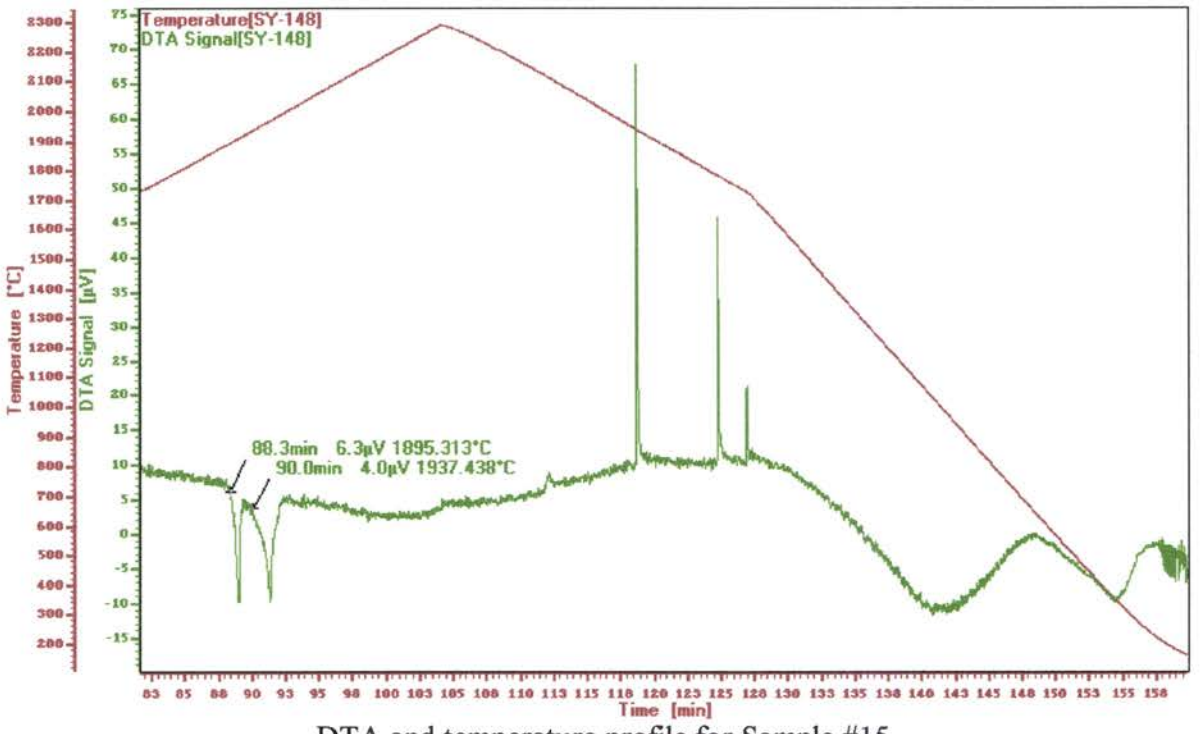

DTA and temperature profile for Sample #15

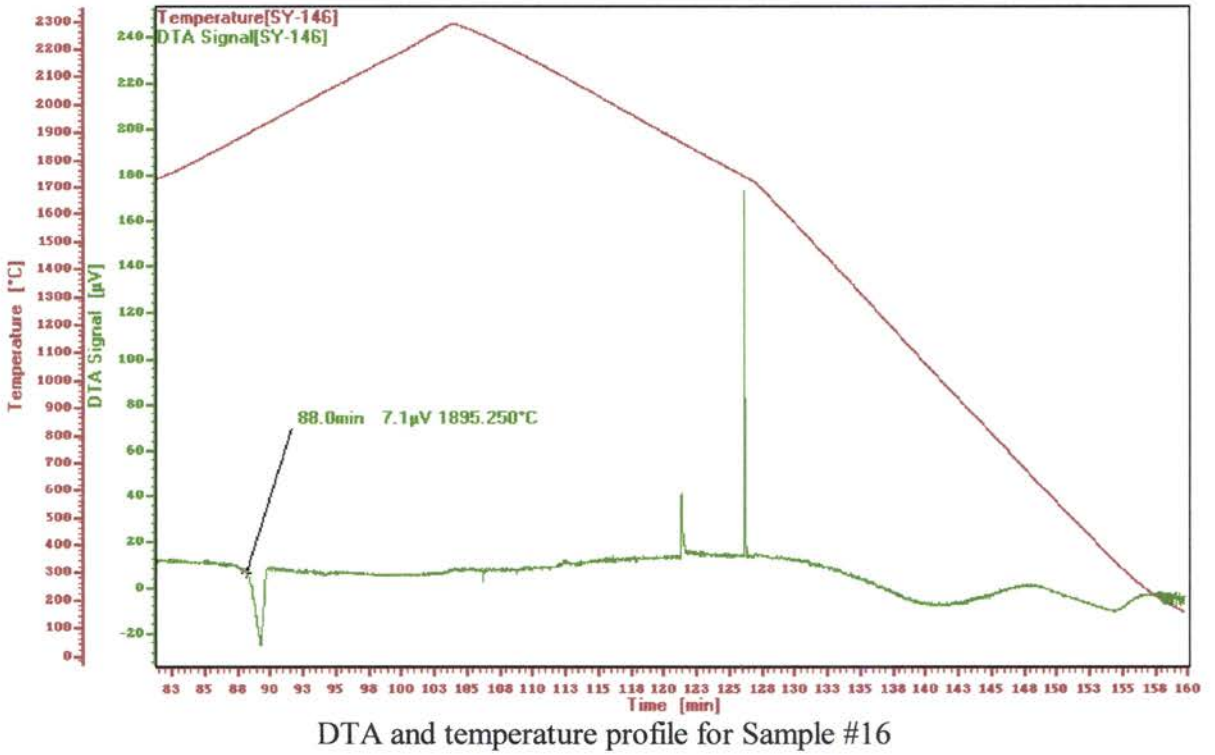

DTA and temperature profile for Sample #16

APPENDIX II: EXTRAPOLATION OF EQUILIBRIUM MELTING TEMPERATURES FROM DTA RESULTS

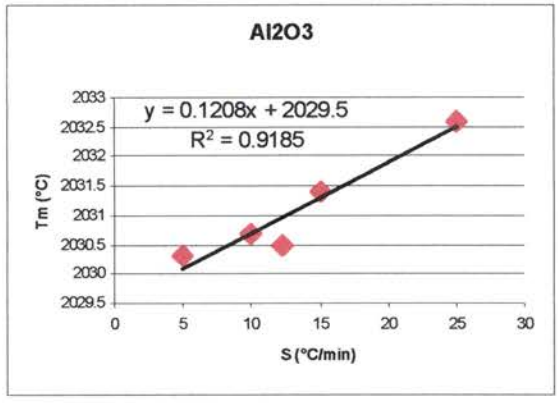

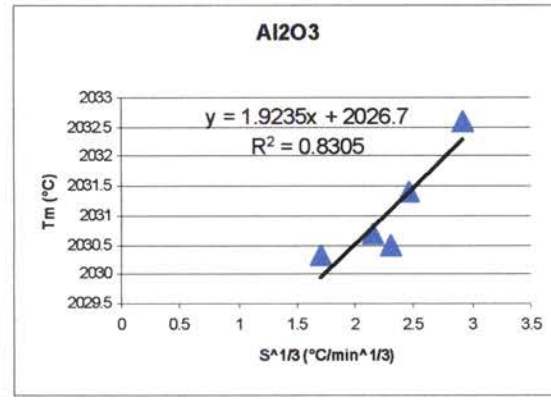

Extrapolation for equilibrium melting temperature for Al_2O_3

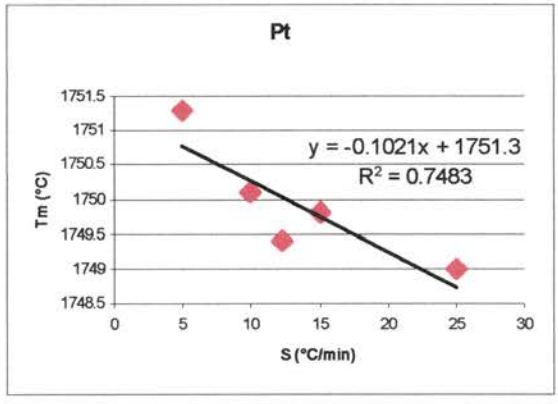

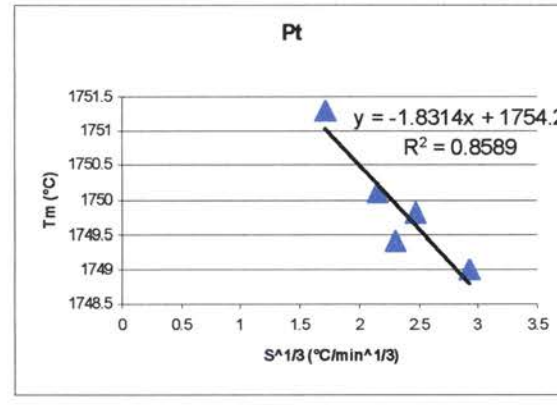

Extrapolation for equilibrium melting temperature for Pt

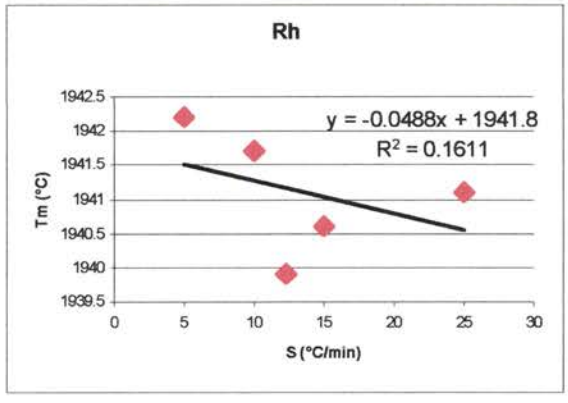

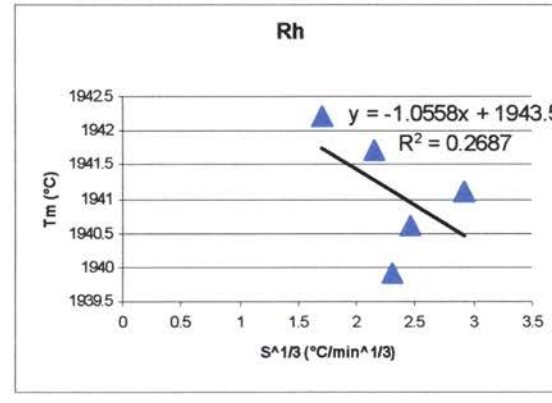

Extrapolation for equilibrium melting temperature for Rh

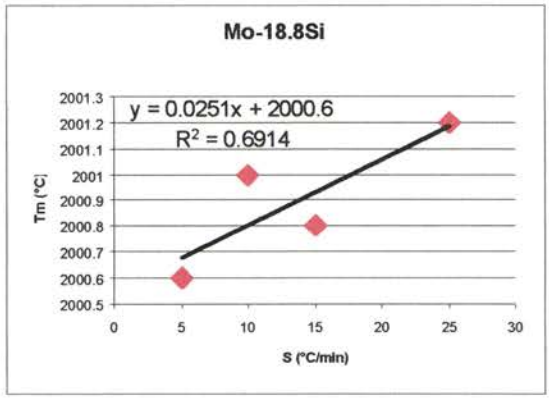

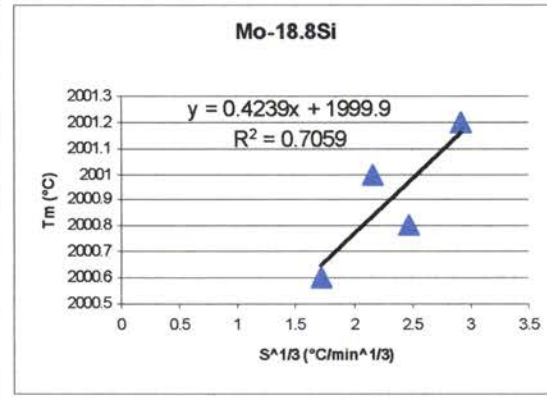

Extrapolation for equilibrium melting temperature for Mo-18.8Si

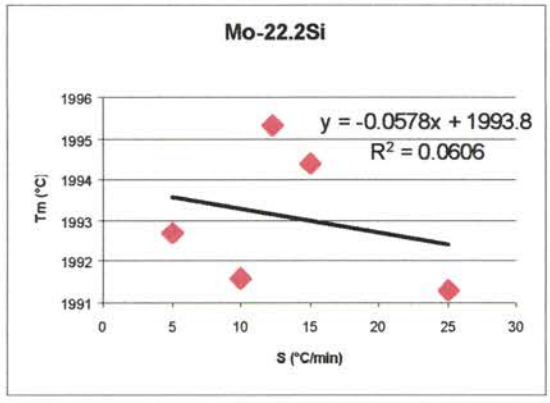

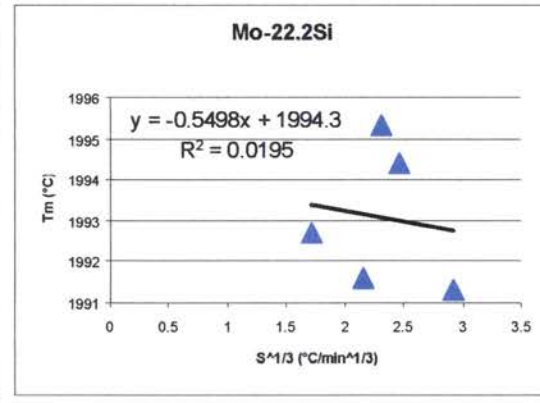

Extrapolation for equilibrium melting temperature for Mo-22.2Si

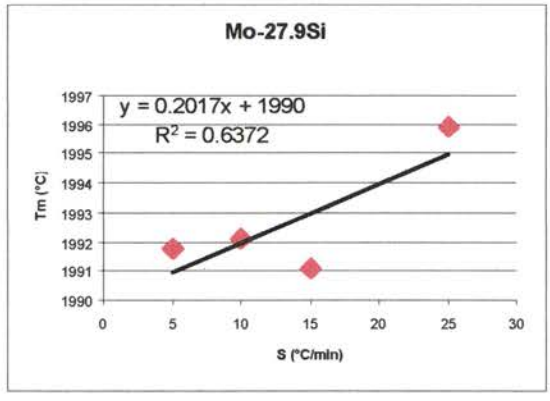

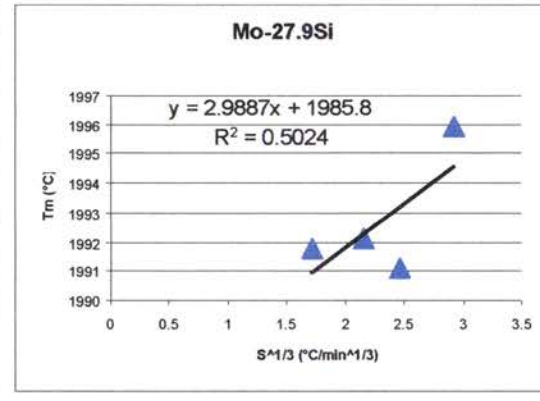

Extrapolation for equilibrium melting temperature for Mo-27.9Si